2011-09-22

Toward the Design of a Statically Balanced Fully Compliant Joint for use in Haptic Interfaces

Levi Clifford Leishman
Brigham Young University - Provo

Toward the Design of a Statically Balanced Fully Compliant Joint

for use in Haptic Interfaces

Levi. C. Leishman

A thesis submitted to the faculty of
Brigham Young University
in partial fulfillment of the requirements for the degree of

Master of Science

Mark B. Colton, Chair
Larry L. Howell
Brian D. Jensen

Department of Mechanical Engineering

Brigham Young University

Thesis Completed September 2011

ABSTRACT

Toward the Design of a Statically Balanced Fully Compliant Joint
for use in Haptic Interfaces

Levi. C. Leishman
Department of Mechanical Engineering, BYU
Master of Science

Haptic interfaces are robotic force-feedback devices that give the user a sense of touch as they interact with virtual or remote environments. These interfaces act as input devices, mapping the 3-dimensional (3D) motions of the user's hand into 3D motions in a slave system or simulated virtual world. A major challenge in haptic interfaces is ensuring that the user's experience is a realistic depiction of the simulated environment. This requires the interface's design to be such that it does not hinder the user's ability to feel the forces present in the environment. This "transparency" is achieved by minimizing the device's physical properties (e.g., weight, inertia, friction). The primary objective of the work is to utilize compliant mechanisms as a means to improve transparency of a haptic interface.

This thesis presents work toward the design of a fully compliant mechanism that can be utilized in haptic interfaces as a means to reduce parasitic forces. The approach taken in this work is to design a series of mechanisms that when combined act as a statically balanced compliant joint (SBCJ). Simulated and experimental results show that the methods presented here result in a joint that displays a significant decrease in return-to-home behavior typically observed in compliant mechanisms. This reduction in the torque needed to displace the joint and the absence of friction suggest that the joint design is conducive to the methods previously proposed for increasing transparency in haptic interfaces.

Keywords: compliant mechanisms, static balancing, haptics, prescribed spring deflections, pseudo-rigid-body model

ACKNOWLEDGMENTS

I would like to acknowledge and express my gratitude to my lovely wife Allyssa for the love, support, and encouragement she has given me throughout my pursuit of higher education and the many sacrifices she has made so that I could complete this thesis. I thank my two daughters, Chloe and Lacie, for giving me the joy in life that only daughters can bring. I would also thank my parents for their consistent encouragement and guidance they give me. I especially want to thank my father for his willingness to listen to my thoughts on this work and to assist in the manufacturing and testing of the prototypes.

I thank Dr. Colton for his involvement in my masters thesis and his commitment to my learning. I greatly appreciate his patience and support in my pursuit of the many avenues that this work has traveled and that he always made my learning a top priority. Dr. Howell and Dr. Jensen were of great help in understanding and developing many of the concepts in compliant mechanism theory that are presented here and without their insights and critiques this work would not have been possible. I also acknowledge the Department of Mechanical Engineering for their support of this work.

I would also thank Kevin Cole for the many hours he spent in assisting me in learning the skills I needed to complete the many tests and for collecting the data presented in this work. Also I would like to thank Sam Wilding for his willingness to assist me in my endeavors in performing the Finite Element Analysis presented in here.

Finally, I would like to acknowledge the loving support of my Heavenly Father that I have received through this journey to completing my master's degree. Many sweet moments He has given me through inspiration and blessing me with feelings of comfort and confidence as I pursued this path. I look forward to moving onto new challenges in this journey of life with Him as my guide.

TABLE OF CONTENTS

LIST OF TABLES

LIST OF FIGURES

CHAPTER 1. INTRODUCTION

1.1 Motivation

Haptic interfaces are force-reflecting devices that provide a sense of touch to users as they interact with virtual or remote environments. The interface acts as an input device, mapping the 3-dimensional (3D) motions of the user's hand into 3D motions in a slave system or simulated virtual world. These devices differ from other computer interfaces in that they have the ability to empower the user with the sense of touch in the environment they are exploring.

The forces and torques that the interface transmits to the user are produced by actuators placed on the mechanism with which the user interacts. Figure 1.1 shows a commercially available haptic interface that has been used in varying applications from surgical robots to video gaming. These interfaces have become wide spread and effective in improving the user's experience in many of the applications in which they are implemented.

Recent advances in computing and control sciences have allowed haptic interface technology to be more effectively used in virtual and remote environments. However, many challenges still limit the technology's ability to be more widely implemented. One major challenge is to ensure

Figure 1.1: Commercial haptic interface used in wide varying fields of applications from gaming to medical simulations

that the forces and torques that the user experiences accurately represent interactions with the remote or virtual environment. Forces and torques that deter from the realistic feel of an environment are seen as parasitic forces and their presence is said to decrease the haptic interface's transparency [1, 2]. The transparency of a typical haptic device can be defined as the accuracy with which the measured forces match the expected forces. It is useful to quantify the transparency G_T as the ratio of the transmitted force to the user, F_m, and the force that the environment experiences [3],

$$G_T = \frac{F_m}{F_e}, \tag{1.1}$$

F_e, where the ideal ratio is one.

How close this ratio is to unity greatly depends on the design and physical parameters of the haptic interface. For instance, the five-bar haptic interface shown in Fig. 1.2 has a highly varying force output dependent upon its link lengths, mass, inertia, friction, and actuator dynamics. This output force,F_m, for the device can be expressed as

$$F_m = f(m_1, m_2, m_3, m_4, I_1, I_2, I_3, I_4, L_1, L_2, L_3, L_4, b_1, b_2, b_3, F_e) \tag{1.2}$$

where m_i is the mass, I_i is the inertia, L_i is the length of a link, and b_i is the damping coefficient in a pivot. This equation illustrates the important role of the interface's physical design in how the interface transmits forces. In order to achieve perfect transparency, the effects of all of the physical parameters in Eq. 1.2 need to be eliminated or compensated in some manner to allow for the $F_e = F_m$. One method of doing this is in the control of the haptic interface. These control schemes require that the parameters are measured or estimated. If perfect estimation of the parameters is achieved and if the control law compensates for the parameters perfectly, $F_e = F_m$. However, all of these parameters require some form of measurement or estimation, which introduces a level of error into the system. This results in a measured force that differs from the force of the environment, leading to inaccurate force information being presented to the user.

Forces that greatly contribute to this deterioration of realistic force information being transmitted to the user are friction, the interface's physical dynamics (weight, inertial forces, compliance), actuator dynamics, and the presence of nonlinear forces as a result of backlash and play in the device's bearings and gears. While control schemes have proven useful to counteract the

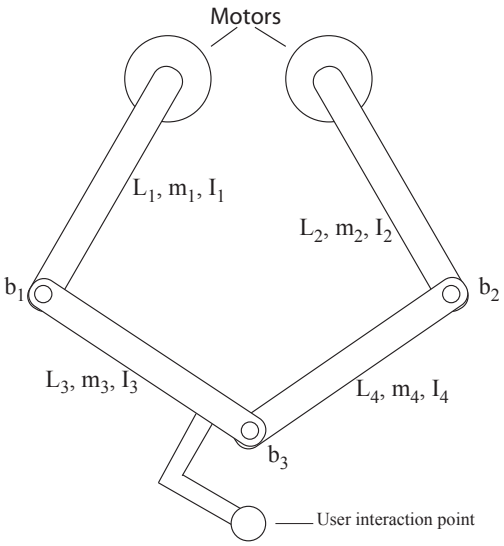

Figure 1.2: Five-bar mechanism often used as a haptic interface. The user interacts with a simulated or remote environment through the user interaction point and forces are transmitted to the user via the motors.

effects of these parasitic forces, it is difficult to accurately model and predict all of the parasitic forces present in a haptic interface. Thus proper design of the device is critical in achieving an interface that exhibits realistic representations of the simulated environments.

A recent approach to mitigate the effects of parasitic forces that are present as a result of bearings in a device is to replace them with compliant mechanisms [3, 4]. This approach removes friction and the play that is present in bearings. These mechanisms also introduce another parasitic force as a result of the compliant joint's restoring torque that is present at any deflected position. While this force can be accurately modeled and compensated for through control methods, it requires additional torque from the motors to do so and thus decreases the available bandwidth of the force output of the device.

Another approach used to compensate for parasitic forces in haptic interfaces is to add additional masses to the mechanism at calculated positions to balance the gravitational forces felt as a result of the device's weight [5, 6]. This approach has shown to be successful in creating a gravity compensated device but displays larger inertial forces as a result of the additional masses. Another form of static balancing exists that has been influential in reducing inertial forces through the use of springs to balance the mechanisms. This approach is capable of achieving the same level

of gravity compensation as the mass balancing approach, and has proven to be easier to control, displays less over-shoot, and faster settling time compared to the mass balancing systems [7].

A solution to the total reduction of parasitic forces in haptic interfaces lies in the combination of compliant mechanisms and static balancing. Recently work in the field of Statically Balanced Compliant Mechanisms (SBCMs) has shown that mechanisms that utilize additional compliant members can be used to balance or counteract the restoring torques in an existing compliant mechanism so that it displays a statically balanced behavior. Implementing these types of mechanisms into haptic interfaces would then allow for the benefits of compliant mechanisms to be inherent in the interface without the drawback of the "return to home behavior". These SBCMs promise to solve many of the problems that face improving the transparency of haptic interfaces as it proves to be a marriage of the two aforementioned approaches already implemented to achieve this goal. The compliant mechanism eliminates the friction and play due to tolerances and wear of traditional joints. The balancing work of the springs will remove the drawback of the compliant mechanism's return to home behavior as well as the gravitational forces that may be present without the significant increase in inertial forces that accompanies mass balancing.

A generic statically balanced mechanism, of useable size and that could maintain a high level of off-axis stiffness, may allow for the level of transparency that can be achieved in haptic interfaces to be greatly increased. The use of SBCMs as a joint could be expanded also into other areas that could benefit from the static balancing and elimination of friction, including general robotics, micro-electro-mechanical systems (MEMs), and surgical applications [8].

1.2 Related Work

1.2.1 Design for Transparency in Haptic Interfaces

The design of haptic interfaces is a subset of the field of robotics and thus maintains many of the same design criteria. However, due to the "human in the loop" control schemes that are implemented to allow for remote or virtual sensing, there are additional design aspects that must be given careful consideration.

Remotely controlled (teleoperated) robotic master slave systems have given much insight into haptic interface design as they often incorporate haptic feedback into these applications. Like

haptic interfaces, these systems require a high level of transparency and accuracy so the operator can perform a task more intuitively. One of the main criteria for such systems is that the position of the master (in our case the haptic interface) correctly represent the position of the slave (virtual environment or some remotely operated robotic system) [1, 9]. This is a critical requirement because improperly represented positions given to the user can be devastating in highly sensitive environments in which teleoperated technology is implemented such as surgical procedures or handling of highly sensitive materials/items.

Additional criteria include a minimum workspace, force and position bandwidth, maximum velocities, accelerations, inertial effects, and gravitational balance of the haptic interface [1,9,10]. Inertial effects and gravitational balance of the device are particularly important because if these forces are too dominant the user will experience unwanted levels of fatigue. Due to human's high sensitivity to small levels of change in force and vibrations (100 Hz -1KHz), the bandwidth, velocity, and acceleration benchmarks are set so that the interface is capable of rendering such forces [2].

Improvement of control methodologies and sensing technologies have greatly enhanced haptic interface performance in responsiveness, stability, and realistic force rendering [2,9,11,12]. One commonly applied approach is to account for damping by integrating a negative damping term into the control to cancel out any physical damping that is present [2]. However these approaches rely on estimations of physical parameters that are difficult to estimate and characterize due to non-linearities (stiction, friction) and changing values of the damping as a result of wear and variable loading conditions.

Another approach to the design of more transparent haptic interfaces is the optimization of the robotic mechanism to minimize parameters that have the largest impact on the "feel" of the mechanism. Mechanisms have been optimized such that their kinematics and the reaction forces at the joints display minimal friction and inertial effects [13]. Optimization techniques have been used to optimize linkages so that a larger workspace with improved force response is obtained with minimal link lengths and masses [14]. Static balancing of the mechanism through the addition of masses has been used to meet the gravitational balance requirement [5,6], but unfortunately , this also increases the inertial effects of the interface.

A more recent approach taken in improving haptic interface transparency and accuracy is the implementation of what is termed compliant mechanisms. These mechanisms obtain all or most of their motion through the compliance of the linkage. Mechanisms that are fully compliant (all motion is the result of the part's compliance) display no friction or backlash [15]. O'Modhrain [16] developed a two-axis haptic mouse that employs flexible linkages; it was found that the flexures had inherent high resonance structural frequencies that limited the bandwidth of the device's force feedback display capabilities. Lawrence [3] used a cable-driven flexible member to act as a frictionless linkage and to generate forces by utilizing its energy storage capabilities. Gillespie [4] created a 2-DOF pantograph-type haptic device that replaces typical bearings with open-cross revolute (OCR) compliant joints. In both [4] and [3], additional control methods and actuation torques are required to compensate for the forces generated by the flexed members to achieve transparency throughout the device's range of motion.

1.2.2 Design of Statically Balanced Mechanisms

A statically balanced mechanism (SBM) is one that is able to maintain static equilibrium without applied actuator torques or forces in any given position of the mechanism. The design of general SBMs has focused primarily on counteracting link weights (gravity compensation) through use of counterweights, cams, linkages, or springs (also called equilibrators) [8, 17, 18]. SBMs have also been developed to maintain equilibrium in the presence of forces and torques arising from springs or other flexural elements in the mechanism, with the objective of eliminating or lessening the fraction of the actuator's effort that is used to overcome the spring forces or torques. This has also been accomplished using counterweights, cams, linkages, or additional springs [19–22].

In the field of robotics, static balancing via the addition of masses has long been applied to achieve a level of gravity compensation in order to reduce the output of the actuator needed to drive the robot. It has been shown that the use of springs can achieve the same balancing without having as great an effect on the system's inertia. Gopalswamy [23] explored the use of torsional springs for gravity compensation, although the approach did not provide perfect balancing. Subsequent work explored adjustable balancing to account for varying loads and configurations [24]. Carr showed that spring-balanced systems required less control effort and overall better control performance compared to mass-balanced systems in response to step inputs [7].

Recently, work related to the field of statically balanced compliant mechanisms (SBCM) has brought new mechanism designs that display static balancing and methodologies related to their design [8, 25–31]. The designs for statically balanced mechanisms consist of compliant grippers [8, 31], and concepts for statically balanced MEMs (SB-MEMs) [28]. Approaches for the design of SBCMs include rigid-body-replacement, building blocks, and structural optimization [30].

A specific area of SBCMs is the design of a statically balanced compliant joint (SBCJ). These compliant mechanisms approximate the motion of rotary joints and display some range of static balancing. Jensen [29] created a SBCM that, while not fully compliant, acts as a rotary joint and displays static balanced behavior over a range of ± 60 degrees. The design is compact and is easily manufacturable. Morsch [25] presented the design of a zero stiffness joint (ZSJ) that displayed approximately 70% moment reduction and displayed a range of ± 30 degrees of static balancing. However, this design had a footprint of approximately 0.0256 m^2 and a width of 0.4 m. While the design displayed acceptable range and balanced behavior, its size greatly prohibits its use in functional mechanisms. An approach taken for the design of SBCJ's is to use SBMs as a starting point [25]. This approach requires the use of non-linear springs to replace the zero-free-length springs traditionally used in the SBM and work related to that field is presented in Section 1.2.3.

1.2.3 Design of Springs for Prescribed Force/Moment Deflection Responses

The design of springs to achieve desired force-deflection curves is a problem that has been well defined for specific force-deflections such as constant force or constant spring rate. Theory for the design of the helical, washer, beam, and constant force springs have been developed into a well defined science over the last 300 years [32]. The majority of these theories produce springs with constant spring rates or constant force outputs. The spring's deflection range is very dependent on the type of spring that is designed and its undeflected length (free-length). While these designs are extremely useful, they are unable to meet the needs of applications that require a specific nonlinear force-deflection response or that have limited physical space available for the spring with the desired deflection range to be implemented.

The physical space a spring requires is a challenge that can be overcome in many designs through the use of pulleys and offset springs [18]. The addition of the pulleys and cables that

attach the spring to the system add friction and compliance that is difficult to quantify. The effects of a pulley system reduce the overall effectiveness of the spring and are undesirable in precision applications. There are also many applications in which this method is unfeasible due to challenges with manufacturing. For example, MEMS provide a special challenge due to their size and method with which they are manufactured. Many traditional theories for spring design are not easily transferred to the design of springs to be used in MEMS, and manufacturing MEMS springs based on traditional theories may be impossible.

Compliant mechanisms have proven useful in spring designs that require small free-lengths and large deflection ranges [33–37]. The spring designs have been produced using the two leading design methodologies for compliant mechanisms: the Pseudo-Rigid-Body Model (PRBM) and structural optimization methods. These approaches have led to the creation of new types of springs with useful force-deflection relationships, as well as the capability to specify a prescribed force-deflection response using the structural optimization techniques [36, 37]. While it has been shown that the Pseudo-Rigid-Body Model can be utilized to design constant force springs [34], little has been done to outline a methodology that can be used to generate compliant mechanism springs for any prescribed force-deflection response based on the PRBM.

The capability to optimize a spring for a given force-deflection is apparent in structural optimization methods, and can be completed through the construction of the proper objective function. Other methods have been presented and have recently been revisited in which optimization routines are used to design compliant mechanism springs with distributed compliance for prescribed force-deflection responses. Parkinson [38] presented a parametric approach to the design of compliant mechanisms using splines as the design elements being analyzed in a finite element analysis (FEA) package. Compliant mechanism designs that yielded constant force and prescribed path following were demonstrated. More recently Jutte expanded the idea of using splines as the design element for a compliant mechanism spring into a methodology for the design of a spring for a prescribed force-deflection response [36, 37]. The method again used a finite element modeling package to compute the objective of the optimization but used a genetic algorithm as the optimization routine. Springs were designed for various force-deflection functions and proved to match the predicted models with a high level of accuracy.

Other methods for the design of a prescribed force deflection response have been used and have yielded designs with rigid segments [26, 34, 39]. In [34, 39] the designs were optimized for a constant force and were not shown to extend to the design of mechanisms for any prescribed force. A building block approach was used in [26] to generate a statically balanced mechanism through the optimization of each element of the design until the output force was zero over the mechanism's range of motion. Only in [34] has the PRBM been utilized for the design of a spring for a given response and did not require the use of a finite element model in the optimization. Rather the PRBM parameters were the design variables for the optimization and the resulting designs were able to approximate the desired force-deflection.

1.3 Approach

In the design of general SBMs, including SBCJs, the level of static balancing and the range of motion over which the mechanism is balanced are highly dependent on the type of springs and how they are integrated into the mechanism [18]. However, in past research related to the design of SBCJs, the type of springs and integration geometry were treated separately. In [25] the spring attachment points and the spring parameters are investigated for a set spring type and in [29] the optimized spring design resulted in a partially compliant statically balanced joint due to the integration of two pivot joints into the design. The approach that is presented here relies on the ability to generate specific designs that result in balancing springs optimized to contribute the necessary moment about the joint for the specified geometry. Thus through the exploration of many different compliant spring designs, two specific spring designs can be created that allow for the balancing of a compliant joint.

To illustrate the approach taken in this work, consider the spring-butterfly mechanism shown in Fig. 1.3. A statically balanced version of the spring-butterfly requires that the net torque (M_{Tot}) about the pivot is zero as the mechanism moves through the angle θ. If an inherent moment exists about the pivot (due to pivot compliance or gravity), creating a statically balanced mechanism requires careful consideration of the connection points of the springs and the springs' stiffness. Whenever pivot compliance is present, the required stiffness of the springs will be of a nonlinear nature so that the proper angle-varying moments are exerted about the pivot to maintain a net moment of zero.

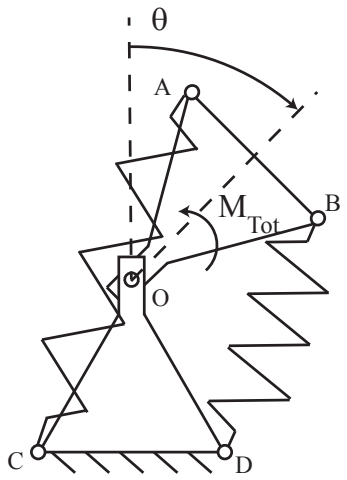

Figure 1.3: A configuration of the spring butterfly mechanism.

For a fully compliant mechanism, the pivot in Fig. 1.3 is replaced by a compliant joint and the coil springs are replaced by compliant mechanism springs, as shown in Fig. 1.4. Again, the springs and spring locations are designed to maintain a total moment of zero about the pivot. For a compliant spring-butterfly as shown in Fig. 1.4, the total moment about the pivot is

$$M_{Tot} = T_{joint} + M_{sp_1} + M_{sp_2}, \tag{1.3}$$

where T_{joint} is the moment due to the compliant joint itself, and M_{sp_1} and M_{sp_2} are the angle-dependent moments about the pivot due to the compliant springs. The nature of T_{joint} depends on the type of compliant joint that is to be balanced. For the joint to be statically balanced, $M_{Tot} = 0$; the compliant springs must therefore be designed so that M_{sp_1} and M_{sp_2} sum to cancel T_{joint} , as shown in Eq. 1.3. The methods for doing this are presented in Chapter 2.

The steps taken for the design of a SBCJ are as follows.

1. Spring 1 is initially specified to have a linear force-deflection curve given by $k * \delta_{sp}$ where k is the stiffness of the desired spring and δ is the spring's deflection from its free-length. The endpoints of spring 1 (points A and C) on the SBCJ are chosen so that the distance between the points is the spring's free-length when $\theta = \theta_{max}$ as shown in Fig. 1.5(a) and $M_{sp_1} = -T_{joint}$ when the $\theta = \theta_{min}$ shown in Fig. 3.2(b).

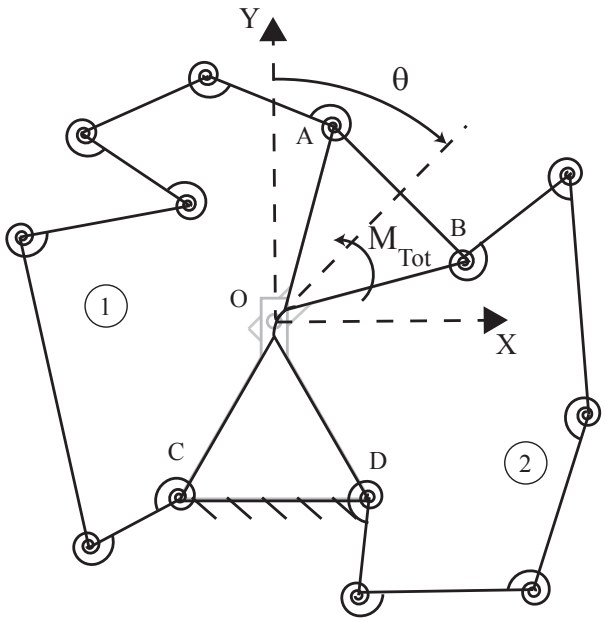

Figure 1.4: Concept for a fully compliant spring butterfly mechanism.

2. With points A and C defined, the spring design is generated using an optimization method that was developed for the generation of spring designs for prescribed loading conditions. The actual moment modeled by the spring's PRBM is then used to find the target moment for the second spring:

$$M_{sp_2} = -(T_{joint} + M_{sp_1}). \tag{1.4}$$

3. The desired moment for the second spring is used as the objective of the optimization and a design for the second spring is obtained using placements of points B and D so that the joint is symmetrical. Figure 1.6 demonstrates what the resulting moments are when the spring designs produce the desired moments.

1.4 Overview of the Pseudo-Rigid-Body Model

The pseudo-rigid-body model (PRBM) was developed as a means in which the motion, force transmission, and energy storage of compliant mechanisms could be modeled using basic kinematic analysis principles. The model is based on simple assumptions of the nonlinear de-

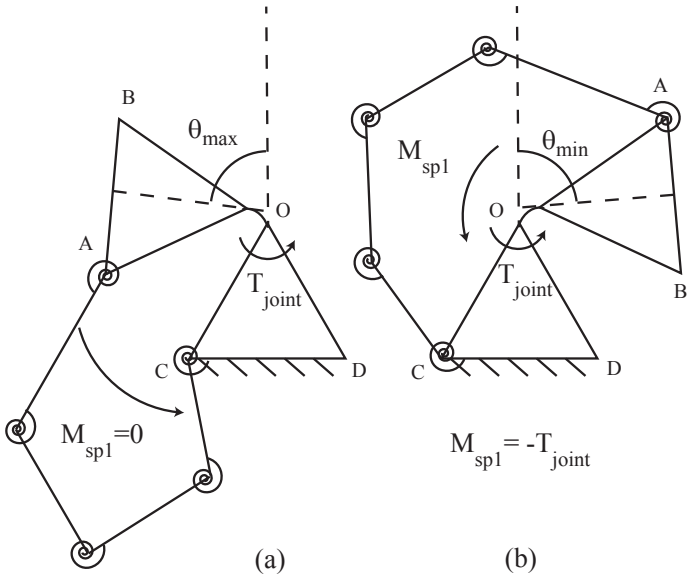

Figure 1.5: Spring 1 attachment on the compliant joint. (a) Attachment position of the undeflected spring. (b) Position of maximum deflection for spring 1.

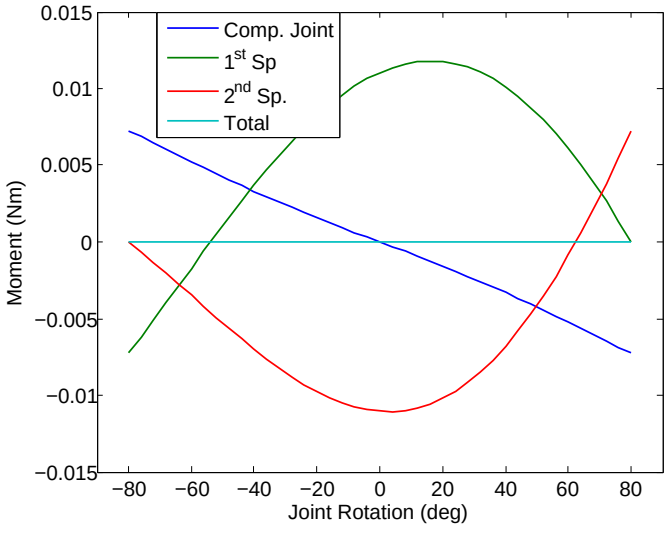

Figure 1.6: Theoretical moment response for a statically balanced joint and its components.

flections of beam type elements, and these assumptions allow for the members undergoing the nonlinear deflections to be represented by rigid bodies and torsional springs.

A principal assumption upon which the PRBM is based is that some point on the member undergoing the nonlinear deflections follows a path that is nearly circular. This point then dictates the length of the rigid link representation of the member and the placement of the torsional spring. Many PRBMs have been developed for varying elements undergoing large deflections and a list of basic representations is found in [15], along with the development of the equations associated with those PRBMs. The compliant mechanism springs designed and implemented in this work all follow the PRBM for the small length flexural pivot and the development of its model and calculations is presented here.

1.4.1 Small Length Flexural Pivots

A small length flexural pivot is a type of compliant joint that allows for a link to rotate about a point via the deflection of a relatively small segment of the link compared to its overall length. Figure 1.7 depicts a small length flexural pivot, its PRBM and their relative positions in a deflected state. It has been shown that the link's end will closely follow a circular path as it deflects and the center of the circle is located in the middle of the small length flexural pivot [40]. This is the location of the characteristic pivot in the PRBM and the location at which a torsional spring is placed. The angle of the PRBM Θ is equal to the angle of the pivots rigid segment and the stiffness of the torsional spring is expressed as

$$k_T = \frac{EI}{l}, \tag{1.5}$$

where E is the Young's Modulus of the material used in the pivot, I is the area moment of inertia of the flexible segment, and l is the length of the small flexible segment. This model for the small length flexural pivot is most accurate when $L >> l$ [40].

The location of the end of the link can then be found using the parameters of the PRBM. Eqs. 1.6 and 1.7 describe the location of the horizontal (a) and vertical (b) placements of the links end location which are defined as

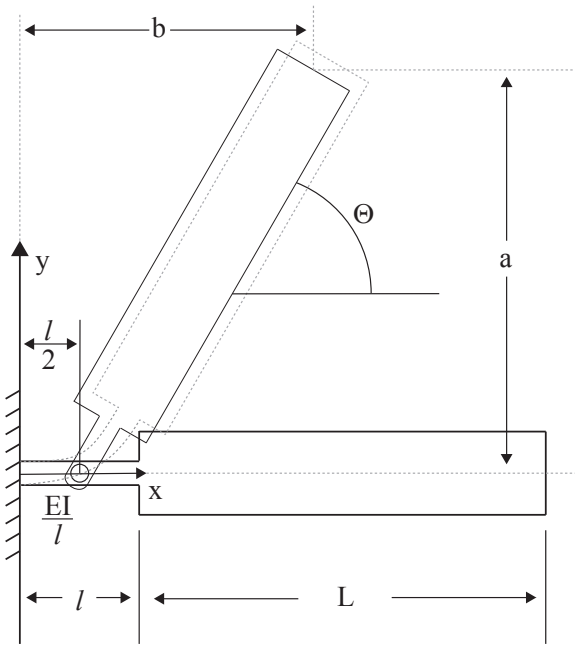

Figure 1.7: A small-length flexural pivot and its pseudo-rigid-body model.

$$a = (L + \frac{l}{2})\cos(\Theta) + \frac{l}{2} \tag{1.6}$$

$$b = (L + \frac{l}{2})\sin(\Theta). \tag{1.7}$$

The stress in the pivot due to the loads applied to the flexure can be expressed in terms of the force loading.

$$\sigma_{max} = \frac{P(a+nb)c}{I} - \frac{nP}{A} \tag{1.8}$$

where the stress can be expressed in terms of the moment load through

$$\sigma_{max} = \frac{6M}{wh^2}, \tag{1.9}$$

where h is the height of the beam and w is the in page thickness of the element. M is equal to the torque generated by the torsional spring at the pivot, which is calculated as

$$T = k_t\Theta. \tag{1.10}$$

Substituting 1.10 into 1.9 we obtain the following stress equation for the pivot in terms of the pivot's stiffness and angle of deflection:

$$\sigma_{max} = \frac{6k_t\Theta}{wh^2}. \tag{1.11}$$

This model and the accompanying sets of equations are the basis of the models presented here for compliant mechanism springs. A more detailed explanation and additional PRBMs can be found in [15].

1.5 Thesis Overview

The work presented in this thesis describes the progress that has been completed towards the design of compliant mechanisms, specifically statically balanced compliant joints, for use in haptic interfaces. The approach taken calls for the design of special compliant mechanism springs that follow prescribed loading deflection curves. A case study showing this point, the development of the spring model, the optimization method, and results validating this work are shown in Chapter 2.

Work on the implementation of the spring's model and optimization routine into a SBCJ is presented in Chapter 3. A model of the compliant joint is given along with an explanation of how the optimization is used to create two spring designs, that when combined with the compliant joint, result in a SBCJ. Results from a prototype SBCJ are given and discussed.

CHAPTER 2. DESIGN OF COMPLIANT MECHANISM SPRINGS FOR USE IN STATIC BALANCING

As a preliminary step in developing SBCJs for use in haptic interfaces, a case study on compliant mechanisms and haptic interfaces was performed. An overview of the case study is given in Section 2.1, and demonstrates the need for the ability to design compliant mechanism springs for prescribed loading conditions. The remainder of the chapter describes methods for modeling and optimizing springs for use in SBCJs. A model of the springs and and the methods for calculating their outputs in Section 2.2-2.4 is explained in detail, along with examples of their implementation. The optimization routine that was specially developed for the design of the springs is outlined in Section 2.5. Prototype spring designs are presented as well as experimental characterization results, in section 2.6. The chapter concludes with a discussion on the effectiveness of the model along with its limitations and shortcomings.

2.1 Case study on the Feasibility of Compliant Haptic Interfaces

A device that has the characteristics of perfect static balancing is the spring butterfly [18] (Fig. 2.1). This device is in static equilibrium for all values of θ if the device includes zero-free-length springs, meaning that the springs have a length of zero when they are unstretched. Zero-free-length springs have a force $F = kd$, where k is the spring rate and d is the total length of the spring. They differ from typical springs that have a non-zero free length and a force output that is proportional to the total stretch of the spring.

It can be shown that the spring butterfly is statically balanced in any position by summing moments about the point O shown in Fig. 2.1. The spring forces are described by the vectors F_1 and F_2 and can be expressed as

$$\mathbf{F_1} = Kd_1 \frac{\mathbf{r_{g1}} - \mathbf{r_1}}{\left|\mathbf{r_{g1}} - \mathbf{r_1}\right|} \tag{2.1}$$

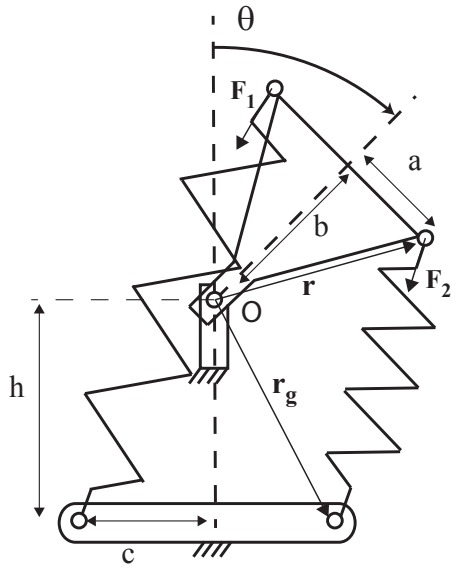

Figure 2.1: Spring butterfly shown in the horizontal plane. This mechanism is statically balanced for any value of θ if the springs are zero-free-length springs.

$$\mathbf{F_2} = Kd_2 \frac{\mathbf{r_{g2}} - \mathbf{r_2}}{\left|\mathbf{r_{g2}} - \mathbf{r_2}\right|}, \tag{2.2}$$

where d_1 is the deflection of spring 1, d_2 is the deflection of spring 2, $\mathbf{r_1}$ and $\mathbf{r_2}$ are the locations of the attachment points of spring 1 and 2 on the pivot link, $\mathbf{r_{g1}}$ and $\mathbf{r_{g2}}$ are the locations of the attachment points of the springs on the base link. The total moment about O is found from

$$M_O = \sum \mathbf{M} = \mathbf{r_1} \times \mathbf{F_1} + \mathbf{r_2} \times \mathbf{F_2}. \tag{2.3}$$

By substituting Eq. 2.1 and Eq. 2.2 into Eq. 2.3 and completing the cross products results in the following equation for the moment about O,

$$M_O = 2Kbh[\sin\theta - \sin\theta] = 0. \tag{2.4}$$

A small haptic interface was designed using the spring butterfly model and compliant mechanism springs to test the design of a statically balanced mechanism using compliant parts. The linear springs shown in Fig. 2.1 were replaced by zero-free-length compliant springs, as shown in Fig. 2.2.

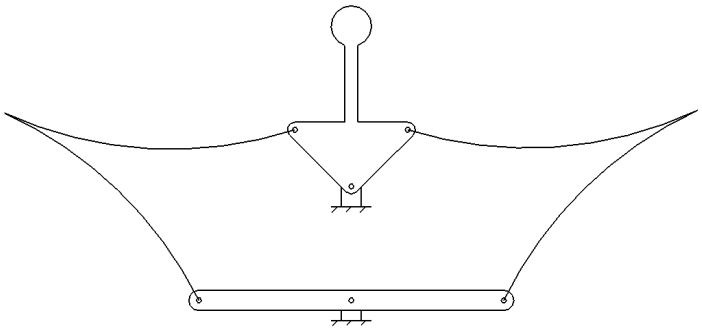

Figure 2.2: Schematic diagram of the haptic device with compliant zero-free-length springs.

In the design,the compliant beams shown in Fig. 2.2 can be represented as linear springs as those shown in Fig. 2.1. Since the compliant members are connected by pins at two endpoints only, the force generated by flexing the members must act along the line connecting the two joints. The compliant springs have zero-free length (the beams can close completely), and so, the springs will always exert tensile forces to attempt to bring the inter-joint distances to zero. Since they are zero-free-length springs, they may be used in the spring butterfly configuration to result in static balancing.

Like a linear spring, the forces from these springs are functions of the displacements of its members. The challenge is to determine the force-deflection relationship for the compliant members shown in Fig. 2.2. The PRBM approach allows us to determine the force-deflection relationship by replacing deflection of compliant members by an equivalent rigid body rotation. The PRBM for the upper half of one of these springs is shown in Fig. 2.3. It consists of a rigid link attached to ground through a pin joint and torsional spring. The length of the rigid link is 85% of the length of the compliant member, and the pivot point is located on a cantilevered section whose length is 15% of the length of the compliant member. As the beam bends, the endpoint closely follows a circular arc about this pivot for pseudo-rigid-body rotations of $\Theta \leq 60$ degrees, where

$$\Theta = \arcsin \frac{d}{2L\gamma}, \tag{2.5}$$

and d is the distance between the two ends of the spring, and γ is the characteristic radius factor (in this case, $\gamma = 0.851244$). The equivalent torsional spring resists bending with a spring rate K_t

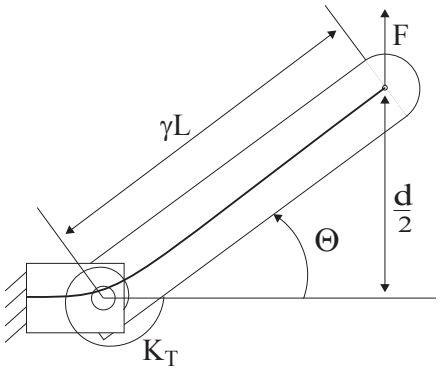

Figure 2.3: Pseudo-rigid-body model for a cantilever beam.

calculated from

$$K_T = \gamma K_\theta \frac{EI}{L} \tag{2.6}$$

where K_θ is the stiffness coefficient (K_θ = 2.6743) for the vertical loading condition shown in Fig. 2.3 [15]), E is the modulus of elasticity, I is the area moment of inertia, and L is the total length of the beam.

In the case of the prototype haptic device, each spring is represented as two separate links that rotate about a common pivot point (see Fig. 2.4). Using the PRBM, the force generated by this spring is

$$F = \frac{K_t \Theta}{\gamma L \cos\Theta} \tag{2.7}$$

where Θ is found as a function of the total inter-joint deflection of the spring in Eq. 2.5 and K_t is defined in Eq. 2.6.

Since the haptic interface does not use linear springs, Eq. 2.1, 2.2, and 2.3 must be modified to account for the more accurate spring forces predicted by the PRBM. To find the magnitude of the force F required to deflect the springs a distance d, Eq. 2.5 is substituted into Eq. 2.7. After some trigonometric and algebraic simplifications F is found to be

$$F = \frac{2K_t \arcsin\frac{d}{2L\gamma}}{\sqrt{4\gamma^2 L^2 - d^2}}. \tag{2.8}$$

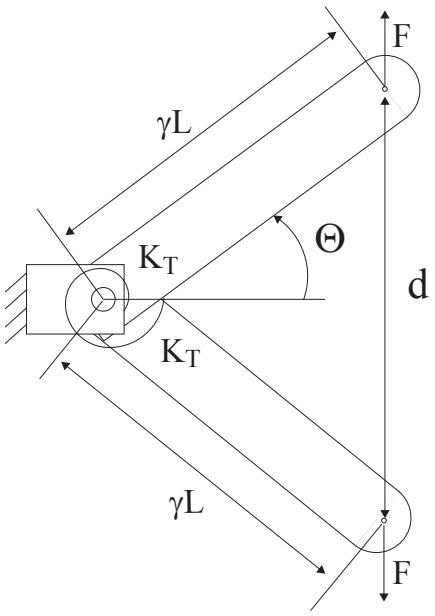

Figure 2.4: Pseudo-rigid-body model for the compliant zero-free-length springs.

Replacing the linear spring force magnitude Kd in Eq. 2.1 and Eq. 2.2 by the PRBM spring force magnitude defined by Eq. 2.8 yields the spring force vectors

$$\mathbf{F_1} = \frac{2K_t \arcsin\frac{d_1}{2L\gamma}}{\sqrt{4\gamma^2L^2 - d_1^2}} \frac{\mathbf{r_{g1}} - \mathbf{r_1}}{|\mathbf{r_{g1}} - \mathbf{r_1}|} \tag{2.9}$$

and

$$\mathbf{F_2} = \frac{2K_t \arcsin\frac{d_2}{2L\gamma}}{\sqrt{4\gamma^2L^2 - d_2^2}} \frac{\mathbf{r_{g2}} - \mathbf{r_2}}{|\mathbf{r_{g2}} - \mathbf{r_2}|}. \tag{2.10}$$

The total moment exerted about O can be calculated by substituting Eq. 2.9 and Eq. 2.10 into Eq. 2.3, resulting in

$$M_O = 2K_t \cos\theta(ah + bc)\left(\frac{\arcsin\frac{d_2}{2L\gamma}}{\sqrt{4\gamma^2L^2 - d_2^2}} - \frac{\arcsin\frac{d_1}{2L\gamma}}{\sqrt{4\gamma^2L^2 - d_1^2}}\right) \tag{2.11}$$

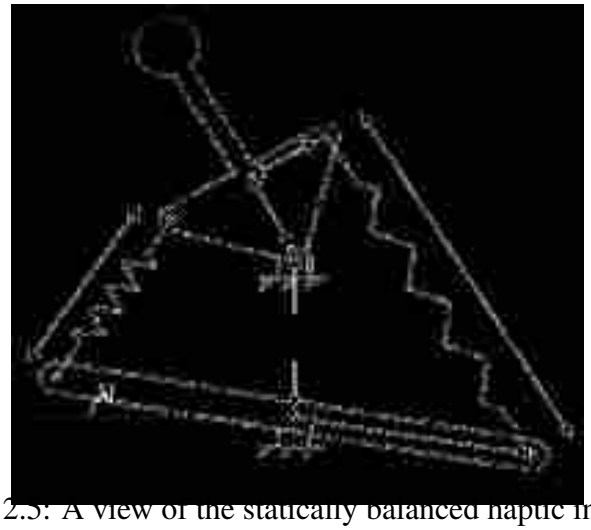

Figure 2.5: A view of the statically balanced haptic interface.

where a, b, c, and h are defined in Fig. 2.5. The lengths d_1 and d_2 are found from the magnitude of the resulting vector of $(\mathbf{r_g} - \mathbf{r})$ and are defined as

$$d_1 = \sqrt{a^2 + b^2 + c^2 + h^2 + 2b(h\cos\theta + c\sin\theta - \alpha) - 2a(h\sin\theta + c\cos(\theta - \alpha) - \frac{hc}{a}\sin\alpha)} \tag{2.12}$$

and

$$d_2 = \sqrt{a^2 + b^2 + c^2 + h^2 + 2b(h\cos\theta + c\sin(\theta - \alpha)) + 2a(h\sin\theta - c\cos\theta - \alpha - \frac{hc}{a}\sin\alpha)}. \tag{2.13}$$

We can see from Eq. 2.11, Eq. 2.12, and Eq. 2.13 that the mechanism will in fact have a zero moment when the input link angle $\alpha = 0$ and the handle angle $\theta = 0$ because at that orientation the spring lengths are equal ($d_1 = d_2$). However in Eq. 2.11 M_O is not precisely equal to zero for all handle angles for the springs used in this device. Fig. 2.6 shows the handle moment M_O when α is held at zero and the handle angle θ is varied. The completed prototype, however, did display a range of static balancing and can be attributed to the small values of the remaining moments about O and the presence of friction in the pin joints. This prototype led to the belief that a fully compliant joint (all motion is obtained through the flexion of the mechanism) could be designed and constructed.

One major requirement however, is that the compliant springs used as the balancing members of the compliant joint need to be specifically designed for such a purpose. These springs

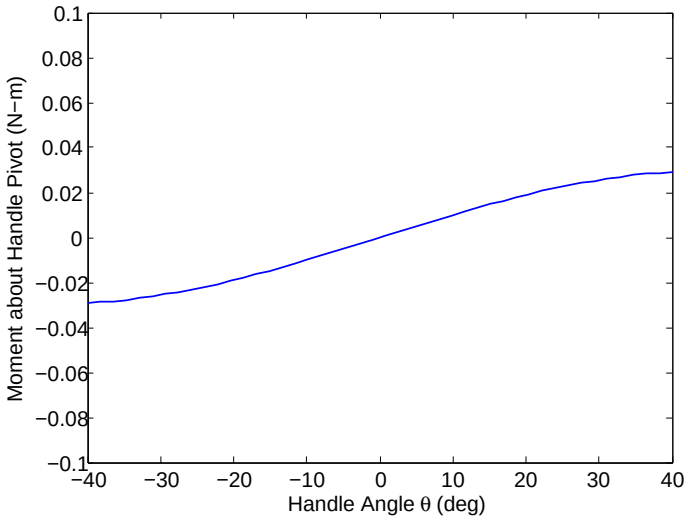

Figure 2.6: The predicted moment of the compliant haptic interface.

need to be able to follow unique force deflection or torque deflection curves in order to achieve a functional joint that maintains static balancing over a wide range of motion.

2.2 Spring Pseudo-Rigid-Body Model

Using the pseudo-rigid-body model to design compliant mechanism springs allows the springs to be analyzed using traditional kinematic relationships and the force and moment output of the mechanism is readily found using either newtonian methods or the principle of virtual work [15]. The compliant mechanism springs that are utilized in this study employ the use of small length flexural pivots at each compliant joint to enable the mechanism to obtain its motion. The PRBM for these mechanisms requires that a torsional spring be placed at the midpoint of the small length flexural pivots and the stiffness of the spring is given in Eq. 1.5.

For the approach proposed here for the static balancing of a compliant joint, the moment produced by the balancing springs needs to be modeled so that it can be optimized to generate the proper spring designs so that the total moment of the joint is zero. PRBM's for translational and rotational springs were developed to test the concept of using the PRBM for the springs. The PRBM for each type of spring is presented here along with a description of the displacement vector that describes the spring's deflections.

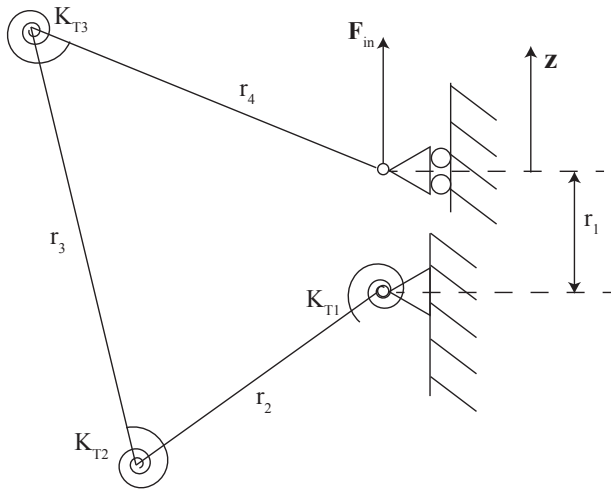

Figure 2.7: The PRBM representation of a compliant mechanism spring with 3 rigid links.

2.2.1 Translational Spring

Figure 2.7 shows the PRBM for a spring with 3 rigid links that undergoes a deflection defined by the displacement **z**. In the case shown, the displacement vector (**z**) is defined so that the end of the spring displaces vertically from its original position. It should be noted that the model is representative of many different types of compliant mechanism configurations as the PRBM allows for various elements to replace the rigid links and torsional springs. In this work however, the springs that are implemented solely utilize small-length flexural pivots.

For every displacement r_1 that the spring can be subjected to there is one position that will have the lowest energy state for the configurations of springs that were investigated. This is where the links in the spring will reside with only a displacement load applied. For the case of the three-link spring shown in Fig. 2.7, the spring resembles a four bar mechanism for any given displacement and will behave as such at each displacement, if the ground link is rigid. The ground link is defined as r_1 and its length is equal to the free length of the spring plus the amount the spring is displaced. The position of each link in the spring can then be found for any given angle of r_2 in reference to the horizontal plane using Eq. 2.14 - 2.19, where $\delta, \beta, \phi, \lambda, \theta_1, \theta_2, \theta_3$, and θ_4 are defined in Fig. 2.8 and

$$\delta = (r_1^2 + r_2^2 - 2r_1 r_2 \cos(\theta_2 - \theta_1))^{\frac{1}{2}} \tag{2.14}$$

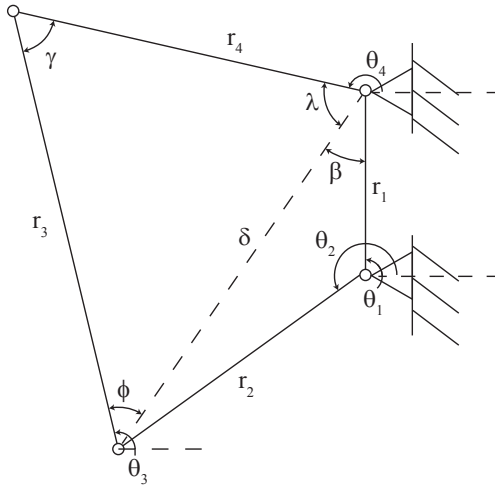

Figure 2.8: Rigid four link mechanism

$$\beta = \arccos \frac{r_1^2 + \delta^2 - r_2^2}{2\delta r_1} \tag{2.15}$$

$$\phi = \arccos\left(\frac{r_3^2 + \delta^2 - r_4^2}{2\delta r_3}\right) \tag{2.16}$$

$$\lambda = \arccos\left(\frac{r_4^2 + \delta^2 - r_3^2}{2\delta r_4}\right) \tag{2.17}$$

$$\theta_3 = \phi - (\beta - \theta_1) \tag{2.18}$$

$$\theta_4 = \pi - \lambda - (\beta - \theta_1). \tag{2.19}$$

A more general PRBM for the compliant mechanism spring is shown in Fig. 2.9, where the number of rigid links in the mechanisms can vary based on the needs of the designer. For this model, vector loop equations are used to solve for the spring's configuration for a given deflection. For the PRBM shown in Fig. 2.9 the vector loop equation can be written as

$$\mathbf{r_1} + \mathbf{r_2} + ... + \mathbf{r_{N-1}} + \mathbf{r_N} = 0 \tag{2.20}$$

where each vector is defined as shown in Fig. 2.9. Equation 2.20 constitutes a system of equations that can be solved to find the spring's undeflected position and serves as constraints in finding the spring's position in deflected positions; the method of doing so will be discussed in Section 2.3.

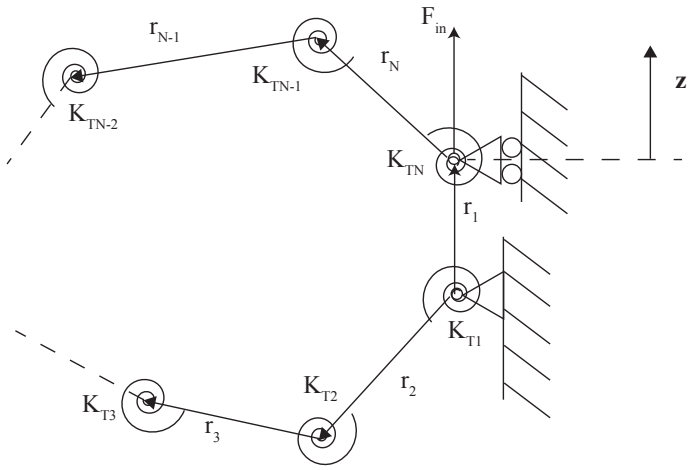

Figure 2.9: A generic representation of the PRBM for a force displacement spring.

2.2.2 Torsion Spring

The PRBM for the torsional springs resembles that of the translational springs and is shown in Fig. 2.10. The two types of springs mainly differ in the displacement that they undergo. For the torsional springs, the displacement that they experience is constrained to follow some path defined by the angle ϕ. As the end of the spring attached to point E is deflected through some angle ϕ, the spring deflects to a new position and exerts a moment (M_{Sp}) about the pivot (H) as depicted in Fig. 2.11.

The position of spring's links can be found using the PRBM. The joint angles θ_n, n=1...N, are found using vector loop equations for the kinematic chain,

$$\mathbf{r_1} + \mathbf{r_2} + \mathbf{r_3} + ... + \mathbf{r}_{N-1} + \mathbf{r_N} = 0 \tag{2.21}$$

where each vector is defined as shown in Fig. 2.10. Equation 2.21 constitutes a system of equations that can be solved to find the spring's undeflected position.

In this study the link angles and lengths were constrained such that the links of the spring would not initially be co-linear and the rotation of the links would stay within the bounds of the PRBM. The spring's undeflected position is defined by specifying $N-2$ link angles and then using Eq. 2.21 to solve for the remaining angles. The spring's link angles at its initial position that are

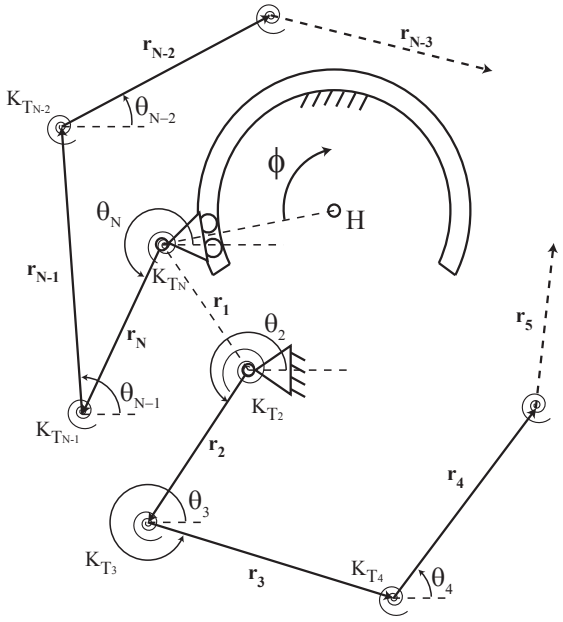

Figure 2.10: The PRBM for a generic compliant mechanism spring.

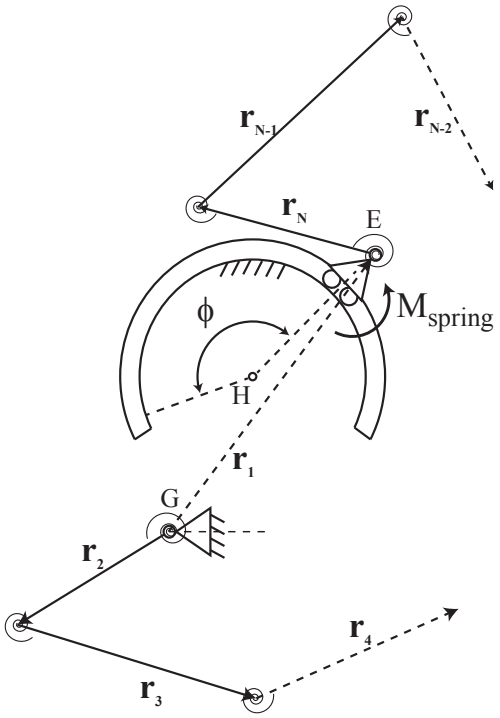

Figure 2.11: The generic compliant mechanism spring in a deflected position.

specified are chosen so that if the number of links, N, is four, the angle of the second link (θ_2) is specified, for $N = 5$, θ_2, and θ_5 specified, and for $N = 6$, θ_2, θ_3,and θ_6 are defined. As N increases, the additional angles that are specified for the un-deflected position are chosen as the next angle in the kinematic chain from its beginning if an even number of links exist and from the end of the chain if an odd number of links are in the chain. These angles are represented as a vector **ANG** which contains these specified angles for the spring's un-deflected position. Additionally, the link length values are represented by a vector $\mathbf{R}$ and the torsional spring constants by $\mathbf{K_T}$.

2.3 Obtaining Spring's Positions in Deflected States

In order to find the position of the spring's links for a given displacement we must search for the minimum potential energy of the spring at each position. The spring will reside at this minimum energy position as it serves as the equilibrium point. The approach taken in accomplishing this task is much like the numerical method presented in [41].

To best describe the method, an example is given for the three-link spring presented in Fig. 2.7. The potential energy of this spring is expressed as

$$V = \frac{1}{2}(K_{T_1}(\psi_1)^2 + K_{T_2}(\psi_2)^2 + K_{T_3}(\psi_3)^2), \tag{2.22}$$

where

$$\begin{aligned} \psi_1 &= \theta_1 - \theta_{1_o} \\ \psi_2 &= \theta_2 - \theta_{2_o} - (\theta_3 - \theta_{3_o}) \\ \psi_3 &= \theta_4 - \theta_{4_o} - (\theta_3 - \theta_{3_o}) \end{aligned} \tag{2.23}$$

and K_{Tn} is the torsional spring constant for the flexible member, θ_n is the deflected angle and θ_{n_o} is the undeflected angle of the n^{th} link. The equilibrium configuration is found by solving Eqn. 2.22 for the angle of r_2 that results in the lowest potential energy with the given displacement. This is done numerically by minimizing the potential energy subject to the vector loop equations as the

constraints. This can be expressed as

$$\begin{aligned} F &= \min_{\mathbf{ANG}}(V) \\ subject \quad to: \\ \sum_{n=1}^{N} \mathbf{r_n} &= 0. \end{aligned} \tag{2.24}$$

This minimization occurs at every increment of the displacement to find the spring's position at that particular deflection.

For the more general case of the spring's PRBM, the potential energy may be expressed as a summation of each torsional spring's potential energy within the spring. For both the force displacement and the moment displacement springs the potential energy is defined as

$$V = \frac{1}{2} \sum_{n=1}^{N} K_{T_n} \psi_n \tag{2.25}$$

where K_{T_n} is the spring constant of the n^{th} spring and ψ_n is the difference between the original angle between two links and the current angle of the links at some deflection for the n^{th} torsion spring.

2.4 Modeling of the Spring's Force and Moment Output

The output force or moment for the springs for a given displacement is found using the principle of virtual work. This method utilizes energy methods to solve for conservative forces acting on a system through the calculation of the virtual work done by a virtual displacement. A brief review of the principles of virtual work as applied to this the spring's presented above is given here.

The virtual work done by an input force $\mathbf{F_{in}}$ over a virtual displacement $\delta\mathbf{z}$, is equal to the force applied over that displacement multiplied with the distance and is expressed as

$$\delta W_F = \mathbf{F_{in}} \cdot \delta\mathbf{z}. \tag{2.26}$$

The virtual work performed by an input moment $\mathbf{M_{in}}$ over a virtual rotational displacement $\delta\phi$ is equal to the moment multiplied by the angle over which it acts and is written as

$$\delta W_M = \mathbf{M_{in}} \cdot \delta\phi. \tag{2.27}$$

The virtual work performed by a spring due to the virtual displacement is defined as

$$\delta W_{sp} = \frac{\partial V}{\partial q} \cdot \delta q \tag{2.28}$$

where V is the potential energy of the spring and q is the generalized coordinate for the system. The total work in the system is found by then summing all of the work completed in the system.

$$\delta W_{tot} = \delta W_M + \delta W_F - \delta W_{sp} \tag{2.29}$$

By inserting in the variables for the virtual work from Eqs. 2.27, 2.28,and 2.26 into Eq. 2.29 the total virtual work performed is found to be

$$\delta W_{tot} = \mathbf{M_{in}} \cdot \delta\phi + \mathbf{F_{in}} \cdot \delta\mathbf{z} - \frac{\partial V}{\partial q}\delta q. \tag{2.30}$$

The force output for the system is found from the total work of the system. This is done by setting Eq. 2.30 equal to zero and solving for the force.

To demonstrate the calculation of the force output of the spring again consider the spring in Fig. 2.7. First the displacement vector is defined in terms of the generalized coordinate r_1. For this spring, $\mathbf{z}$ is equal in magnitude to r_1 and can be defined in terms of the spring's links and link angles as

$$\mathbf{z} = [0, r_2 \sin\theta_2 + r_3 \sin\theta_3 - r_4 \sin\theta_4, 0] \tag{2.31}$$

and the virtual displacement defined by $\mathbf{z}$ is then found by differentiating $\mathbf{z}$ with respect to the generalized coordinate (r_1).

$$\delta\mathbf{z} = \left[0, r_2 \cos\theta_2 \frac{\partial\theta_2}{\partial r_1} + r_3 \cos\theta_3 \frac{\partial\theta_3}{\partial r_1} - r_4 \cos\theta_4 \frac{\partial\theta_4}{\partial r_1}, 0\right] \delta r_1 \tag{2.32}$$

To define the work completed by the spring through the virtual displacement $\mathbf{z}$, Eq. (2.22) is substituted into Eq. 2.28 and the following expression is obtained to define the virtual work of the spring,

$$\delta W_{sp} = (K_{T_1}(\psi_1)\frac{\partial \psi_1}{\partial r_1} + K_{T_2}(\psi_2)\frac{\partial \psi_2}{\partial r_1} + K_{T_3}(\psi_3)\frac{\partial \psi_3}{\partial r_1}) \cdot \delta r_1. \tag{2.33}$$

With the work performed the spring and the virtual displacement defined the remaining unknown is the force required to maintain the displacement. This is found by substituting Eq. 2.26, 2.32, and 2.33 into Eq. 2.29 and recognizing that δW_M =0. The total work is set to zero and the force is found to be

$$F_{in} = \frac{(K_{T_1}(\psi_1)\frac{\partial \psi_1}{\partial r_1} + K_{T_2}(\psi_2)\frac{\partial \psi_2}{\partial r_1} + K_{T_3}(\psi_3)\frac{\partial \psi_3}{\partial r_1})}{(-r_2 \sin\theta_2 \frac{\partial \theta_2}{\partial r_1} - r_3 \sin\theta_3 \frac{\partial \theta_3}{\partial r_1} + r_4 \sin\theta_4 \frac{\partial \theta_4}{\partial r_1})}. \tag{2.34}$$

This expression describes the force required to deflect the three-link spring any given displacement as it is defined in Eq. 2.31 as long as it does not plastically deform any flexible member of the spring. The angles used to find the forces are those found using the minimization of potential energy to find the position of the spring.

The approach for a torsional spring is similar and simplifies to the expression that the moment required to deflect the spring is

$$M_{sp} = -\frac{\partial V}{\partial \phi}. \tag{2.35}$$

where ϕ is the angle through which the spring is deflected about the pivot point H as shown in Figs. 2.10 and 2.11. The derivatives in all of the equations can be found numerically, using Taylor series approximations of the derivatives. For the work completed here the derivatives were calculated using a central difference approximation utilizing the first two terms of the Taylor series [42] and can be expressed as

$$f_i' = \frac{-f_{i+2} + 8f_{i+1} - f_{i-1} + f_{i-2}}{12(h)}, \tag{2.36}$$

where h is the step size of the the data set being differentiated.

2.5 Optimization of the Springs for Prescribed Force or Moment

In the previous section the method of finding the required force or moment to displace a compliant mechanism spring was outlined. With these models in place they can be manipulated so that the designs result in a loading displacement that follows a desired or prescribed curve. The manipulation occurs in the form of an optimization routine that searches the design space of the spring and finds a design that best produces the desired characteristics. The capability to generate these "optimal" designs will aide in the end goal of this work in designing springs that can be used as equilibrators on a compliant joint to obtain a statically balanced compliant joint.

The spring's design space is a complex high degree of freedom system. The order of the system is directly related to the number of parameters that are used as design variables. The number of design parameters is directly related to the number of links that are in the spring design and are represented by the variables **ANG**, **R**, and $\mathbf{K_T}$. For instance the spring with three-links will have 8 design variables (1 link angle, 3 link lengths, 4 torsional spring constants) following the definition of the spring parameters given previously, making it an 8 degree of freedom system. The number of design variables can be quantified as

$$\#DesignVariables = 3(\#RigidLinks - 1) + 2 \tag{2.37}$$

Additional complexity is added to the system due to the kinematic relationships that the design is required to follow and that small perturbations (i.e. in link lengths) may turn an excellent design into an infeasible one (can not be assembled if vector loop constraint is not exactly equal to zero). This complex nature of the design space does not allow for easy location of the optimal designs of a spring for a given objective using gradient based optimizations. Also, the complexity makes it difficult to specify feasible starting points for the gradient based methods. Methods that are used to aide in the exploration of such complex design spaces include the usage of a genetic algorithm.

Genetic algorithms (GA) are designed so that they allow for multiple designs to evolve and compete for selection as the optimal design. The algorithm is patterned after the evolutionary theories used in the life sciences and is dependent upon random processes. Each GA is unique

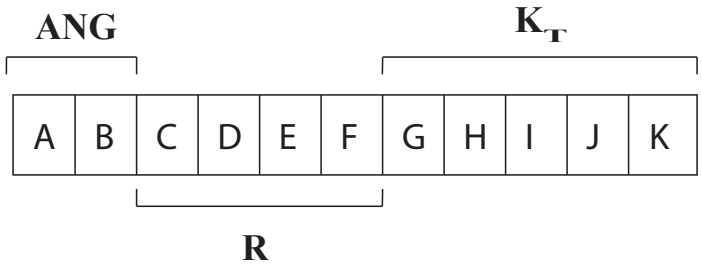

Figure 2.12: Structure of the chromosome for the genetic algorithm. A-K denote the genes of the chromosome and the genes marked by **ANG**, **R**, or $\mathbf{K_T}$ denote the gene comes from that parameter set.

and is designed around the objective of the optimization. Penalty functions are often employed as means to constrain or penalize the designs for undesirable attributes.

In the creation of a GA, one must first specify the parameters of the optimization. These parameters become the genes of the design. All of the genes of a design are ordered and placed in an array-like structure known as a chromosome. Figure 2.12 depicts the structure of the chromosomes used in the optimization of the spring designs for a prescribed loading response. **ANG**, **R**, and $\mathbf{K_T}$ are arrays that carry the parameters of the spring's design as defined previously and the chromosomes grow in length as those parameters increase in size to define springs with higher number of link lengths.

To start the process, a specified number of designs are randomly generated and their objective value is calculated. These designs constitute the population of the first generation of the GA (see Fig. 2.13). These designs can be for any number of link spring. Next the designs go through some level of competition to see which designs will become the parents of the next generation. In the work presented here each member of the population is ranked, with the lowest objective value being ranked a one. The top 25% of the designs in the population are selected to be the parents of the next generation.

The next generation, or the children of the first generation, can be created using various methods. For the work presented here, the methods used are crossover or mutation of the parent's genes. One parent produces three children through these functions. Both of these functions rely on a threshold value (termed crossover or mutation rate) that triggers if the two functions will take place. If none of the thresholds are met through random number selection an exact copy of the parent is produced. A randomly generated number is presented and compared to the crossover of

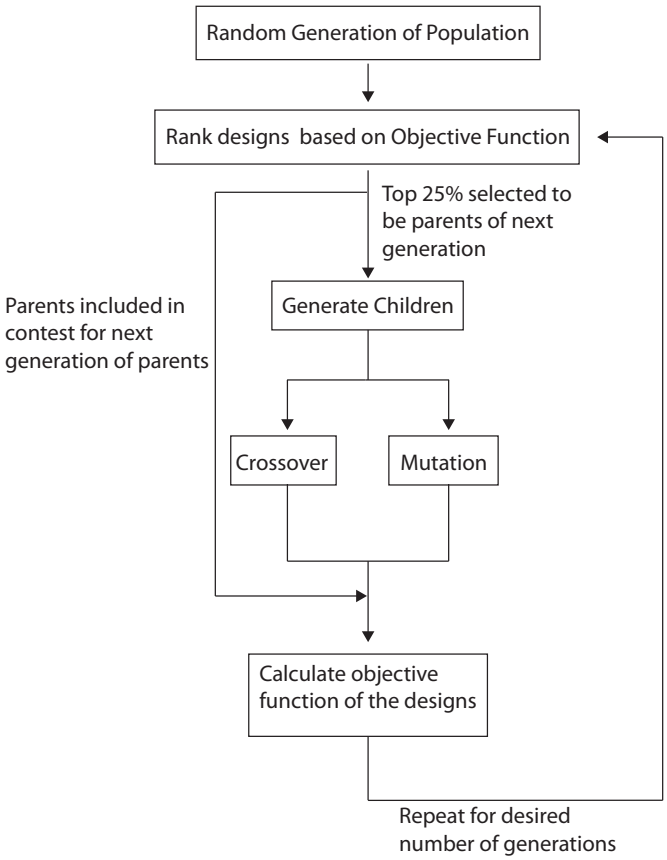

Figure 2.13: A flow chart for the genetic algorithm implemented in the search for spring designs that followed a target loading deflection path.

mutation rates, if the random number is greater than the threshold for a function, the function does not occur. If it is lower, the algorithm begins to calculate which genes to crossover or mutate and the extent of the mutation. Mutation is a random perturbation of the current value of the gene and cross over consists of switching the location of various genes that are of the same type (genes from **R** only crossover with **R** genes)

Table 2.1 shows the differing crossover and mutation rates used for the parameters. It was observed that the algorithm did not perform well with high crossover rates. It was seen that the crossover function typically resulted in designs that were worse in performance, or more commonly, unable to be assembled.

For each parent in a generation, three children were produced. The parents for the next generation are then chosen from the children and the parents. By including the parents from the previous generation a form of elitism is utilized. The process of selecting the next set of parents is that the parent and its children compete against each other and the best of the four designs (1 parent

Table 2.1: Mutation and Crossover Rates for the Genetic Algorithm

Rate	**ANG**	**R**	$\mathbf{K_T}$
Crossover	0.05	0.05	0.05
Mutation	0.4	0.4	0.6

and 3 children) is chosen as one of the parents in the following generation. This competition occurs for each set of parents and children. The entire process is then iterated for as many generations as is specified.

With each generation of the GA the chromosomes are compared against the bounds of the optimization that are set to limit the size and types of spring configurations that where considered. This is to exclude designs that have links that are initially co-linear or that result in links that cross over other links to the extent the mechanism could no longer result in a planar prototype. The parameters that are outside of the bounds are set to be the value of the closest bound. After the completion of the GA the best design is sent to a gradient based optimization to further explore the design space around the GA design. In this sense the GA acts as a filter to the gradient based search, excluding infeasible or poor designs from being a starting point to the optimization.

2.5.1 Optimization Objective Function

The primary objective of the optimization is to minimize the error in the loading-deflection curve of the proposed spring design when compared to the target values. Additional cost functions are added to ensure that the generated spring designs are feasible for manufacturing, functionality, and that the design stays within the limitations of the model that is being optimized. Thus the objective function for the optimization consists of a loading-deflection error function, an assembly cost function, a PRBM limitation cost function, and a stress cost function. It can be defined as

$$F_{obj} = \min_{\mathbf{ANG},\mathbf{R},\mathbf{K_T}} (E_{PO} + E_{ACF} + E_{LCF} + E_{SL}) \tag{2.38}$$

where **ANG**, **R**, and $\mathbf{K_T}$ represent the bounds on the input angles, link lengths, and torsional spring rates for a given spring design. Each individual cost function is outlined in the following sections.

Prescribed Output Error Function

After a spring design's motion is characterized for the deflection it will undergo, its force or moment output is calculated for each given displacement using Eq. 2.30. The error function is then calculated by taking the absolute value of the difference between the desired and actual output of the spring at a given displacement and summing it for each point on the target force-deflection or moment-rotation;

$$E_{PO} = \sum_{i=1}^{m} |P_{des_i} - P_{in_i}|, \tag{2.39}$$

where m is the number of target points specified in the supplied target force-deflection and P is the output of the spring. It should be pointed out that the number of control targets will greatly affect how well the algorithm is able to match the desired output. If the user supplies too few points for a simple function there is a possibility that the algorithm will generate spring designs that exactly pass through the target points but do not behave favorably between those points. Thus the designer must supply a sufficient number of points to adequately define the shape of the force-deflection curve so that the algorithm is constrained to find designs that better approximate the target curve between points with more accuracy.

Assembly Cost Function

Due to the randomly generated designs within the genetic algorithm, there is a possibility that certain designs will not be possible to assemble. Also, certain combinations of link lengths will result in a spring design that will not be able to undergo the desired displacements. In these instances the equations used to define the spring's kinematics begin to be unsolvable, and the minimization in Eq. 2.24 does not converge. In order to avoid such designs the Assembly Cost Function (ACF) is implemented to penalize designs that are impossible to assemble or unable to undergo the required displacements (spring's link lengths are long enough to reach maximum deflection). This function checks if the design does not meet the necessary criteria and assigns a large penalty for the spring design. If either condition is met, the penalty is assessed; otherwise, E_{ACF} is set to zero.

Pseudo-Rigid-Body Model Limitation Cost Function

The PRBM cost function was implemented to ensure that the proposed designs stayed within the limits of the PRBM. According to [15] every Pseudo-Rigid-Body Model is only accurate for deflections less than a certain angle. To account for this a cost function was created that penalized designs that required the PRBM for the spring to have its flexible elements undergo deflections that are outside of the models accuracy limits. For this function the maximum deflection for each joint is found and compared to the limits of the PRBM. If the maximum deflection exceeds the maximum allowable angle of deflection (θ_{max}) the design is penalized proportional to the amount in which each joint angle is greater than θ_{max}. If the joint experiences deflections less than θ_{max}, its cost value is set to zero. The PRBM Limitation Cost Function (LCF) is thus defined as

$$E_{LCF} = \Lambda \sum_{i=1}^{n} (\max(\psi_i) - \theta_{max}) \tag{2.40}$$

where n is the number of joints in the spring design, ψ_i is the difference between the original angle between two links and the current angle of the links at some deflection for the i^{th} torsion spring, and Λ is used to weight the function to the level desirable to the designer. The larger the value assigned to Λ results in a greater cost for the spring's design that exceeds these limits.

Stress Limiting Cost Function

A penalty function was created to penalize designs that required the flexible segments of the spring to experience stress levels that are higher than some percentage of the materials yield strength (YS). To describe this function we look at the bending stress in a beam which can be expressed as

$$\sigma_{max} = \frac{6M}{wh^2}. \tag{2.41}$$

This stress equation can be expanded in terms of the PRBM parameters and written as

$$\sigma_{max} = \frac{6k_t\Theta}{wh^2}, \tag{2.42}$$

where $k_t = EI/l$ for a small-length flexural pivot, which is the flexure type used in the spring. If we expand Eq. 2.42 using the defined values for the small-length flexural pivots and simplify, we

obtain the following expression for the maximum stress in the flexure

$$\sigma_{max} = \frac{Eh\Theta}{2l} \tag{2.43}$$

Examining Eq. 2.43 it becomes apparent that all values of the equation are known except h (thickness of the flexure) and L (length of the flexure). The stress could be easily found if these values were arbitrarily assigned and compared to the stress limit. However this leaves the designer little flexibility in the design of the flexure. The method implemented here is to calculate the stress of the flexure for multiple thicknesses with the length of the flexure set to $0.1L$ (L being the length of the rigid link). All of the smallest stress values for each flexure are then compared to the stress limit

$$S_i = \sigma - \zeta Y S, \tag{2.44}$$

where σ_{min} denotes the lowest stress calculated for the i^{th} flexure using the different thicknesses and ζ is a variable used to scale the yield stress to the desired stress limit. If any S is less than one the value for S is set to zero. Then the stress limiting cost function E_{SL} is calculated by summing the values in S:

$$E_{SL} = \sum_{i=1}^{n} S_i. \tag{2.45}$$

2.6 Testing and Validation

The spring's PRBM proved to be accurate for the modeling of these force and torque outputs of the springs. To test the accuracy of the PRBM various prototype springs were manufactured out of polypropylene. Figure 2.14 shows the predicted moment response of a spring that was modeled using the PRBM method presented here and was constrained to follow a circular path but was not optimized for a specific moment-deflection response. The experimental data taken was taken from the spring shown in Fig. 2.15. Additionally, finite element modeling (FEM) results for the spring are shown. Overall the model is able to predict the shape and magnitude of the spring's moment response well and more accurate modeling is to be expected when using materials with a more linear elasticity. These results allow for confidence that the spring's PRBM would allow for accurate modeling of balancing springs for a statically balanced compliant joint.

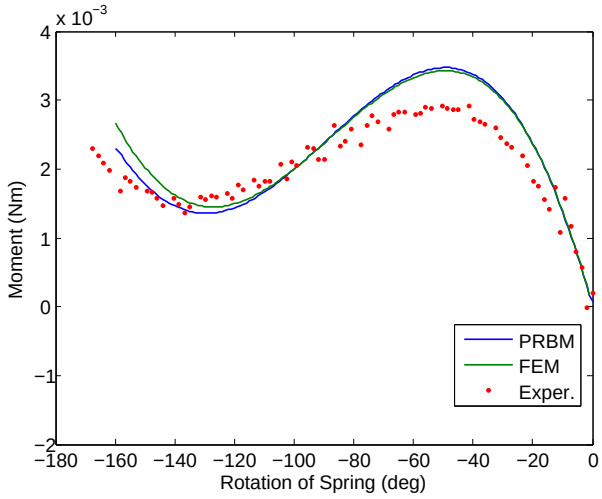

Figure 2.14: The moment response of a compliant mechanism spring designed to follow a circular path.

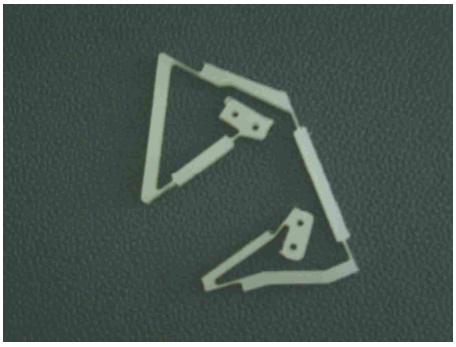

Figure 2.15: A prototype spring designed to follow a circular input path.

Using the the optimization method outlined, spring designs for force displacement and moment displacement springs were generated. The force displacement springs were prototyped and tested for their force response due to a translational displacement on the input point. One spring design is for a three-link spring with a target force-deflection curve that resembles that of a second order spring function defined as $F = Kx^2$. A four-link design was tested with a target function of a spring with a constant spring rate so that $F = Kx$. The final spring design was generated with a target force-deflection for a zero-free length (ZFL) spring. A ZFL spring is a classification of a linear spring that has a force output proportional to its entire length, meaning that it has no physical length when undeflected. Every spring was manufactured out of a polypropylene

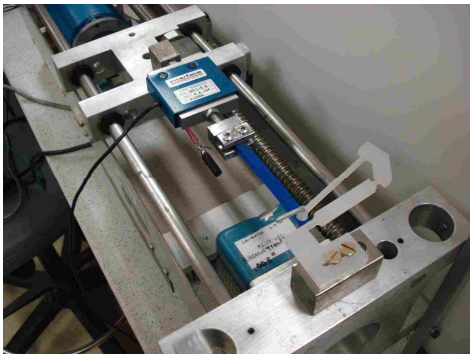

Figure 2.16: The experimental setup for the testing for the spring's force deflection response.

sheet with thickness of 0.00627 m. The designs were tested using a 5 lb load cell mounted on a linear actuator with a position transducer situated on a level counter top as shown in Fig. 2.16. The springs were pulled at a rate of 0.0005 m/s to approximate static displacements. Position and force data were recorded using LabVIEW.

Figure 2.17 shows the response of the three-link spring modeled to be a parabolic spring, and the prototype is shown in Fig. 2.18. Figure 2.19 shows the response for the linear spring in Fig. 2.20. Figure 2.21 displays the results of a compliant mechanism approximating a ZFL spring which is shown in Fig. 2.22. In all of the plots for the force deflection springs it is seen that the magnitude of the springs' responses is less upon their return to their free-length. This is due to the hysteretic behavior of polypropylene. In the case of the three-link spring with a parabolic force-deflection curve in Fig. 2.17 it is seen that the hysteresis is not as prominent. This is due to the low stresses that occurred in this particular spring through its displacement. While each spring displays a high error in their approximations, the shape of the target force-deflection curves are apparent. Table 2.2 displays the specified input angle(s) (**ANG**), pseudo-rigid link lengths (**r**), and the spring constants ($\mathbf{K_T}$) for the springs.

The penalty on spring stresses implemented into the optimization routine proved to be useful in resulting in spring designs that displayed stresses below the specified stress limit. However, at times the resulting designs required that the width of the flexure be extremely large, or small to meet the stress requirement. These designs can often still be implemented as they are, or by the changing of the length and height of the flexure. This is a limitation in the method in which

Table 2.2: Parameters for Prototype Translational Springs

SpringType	**ANG**(rad)	**R** Link Lengths(m)	$\mathbf{K_T}$ Sp. Const.$(\frac{Nm}{rad})$
$F = Kx^2$	pi	0.045,0.045, 0.0545	0.2257,0.0285, 0.08225
$F = K\Delta x$	3.393, 2.753	0.0414,0.0529, 0.0532, 0.0451	0.0845,0.0225, 0.134,0.2274,0.009
$F = Kx$	pi	0.05,0.01, 0.0935	0.01366,0.45, 0.394

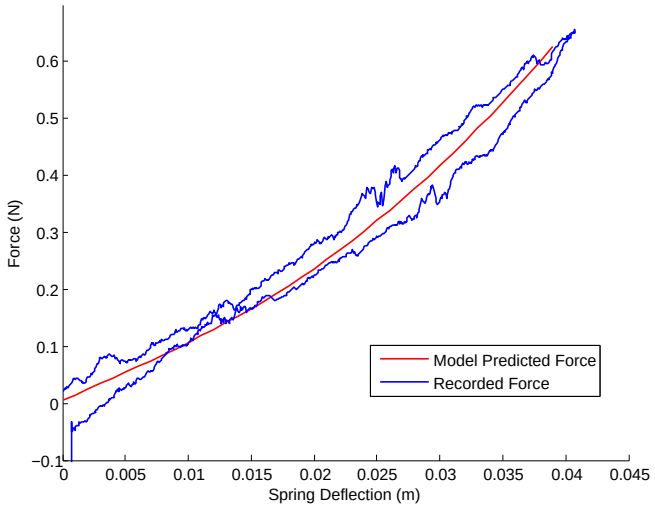

Figure 2.17: Predicted and measured response of a three-link spring designed to display a parabolic force deflection.

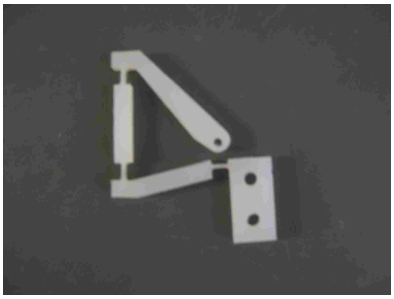

Figure 2.18: Prototype spring designed to approximate a parabolic spring function.

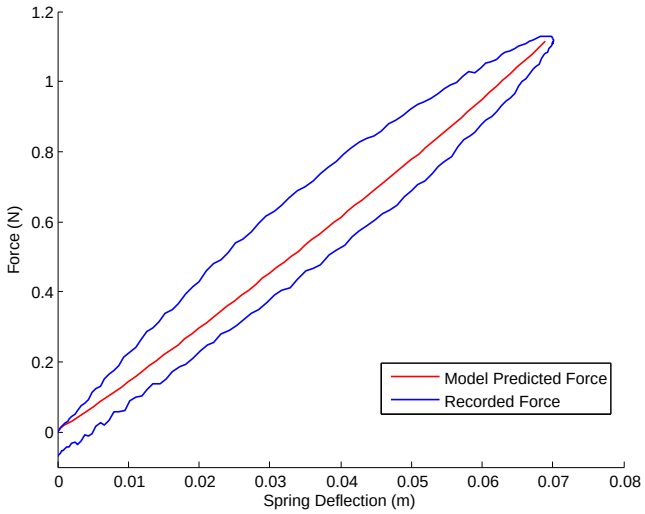

Figure 2.19: Predicted and measured response of a three-link spring designed to display a constant spring rate.

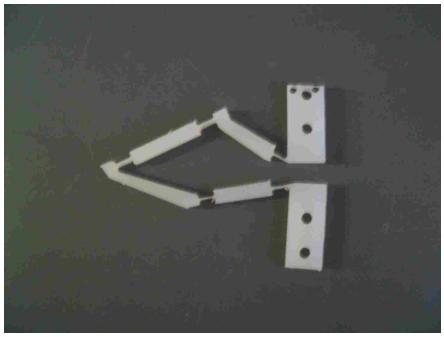

Figure 2.20: Prototype spring designed to approximate a spring with a constant spring rate.

the springs stresses are estimated in the optimization and is potentially a limiting factor to the usefulness of the optimization.

Some of the error in the spring's responses can be attributed to the assumptions made while using the PRBM. The model used in this work assumed that the compressive and tensile loads were such that they do not alter the path that the flexible members follow as they are deformed. The effect of the reaction forces at the pseudo joints may alter the position of the link lengths and the energy stored in the spring. If these forces cause additional deflection of the elements the spring's equilibrium position would change from that which is predicted by the model presented here and affect the accuracy of the force or moment output prediction.

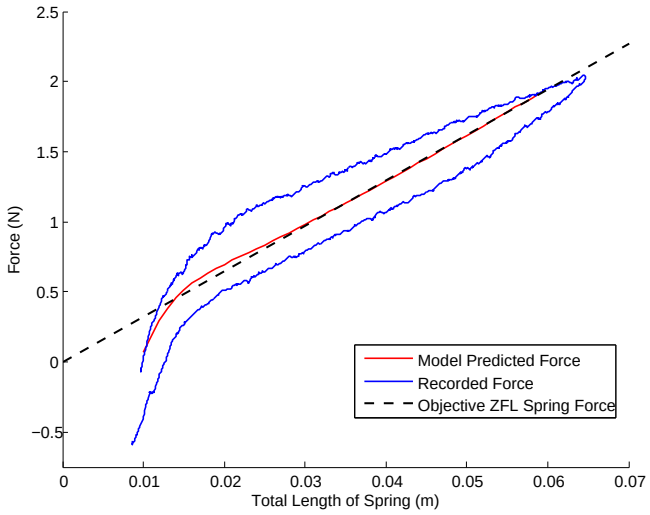

Figure 2.21: Predicted and measured response of a three-link spring designed to approximate a zero-free-length spring.

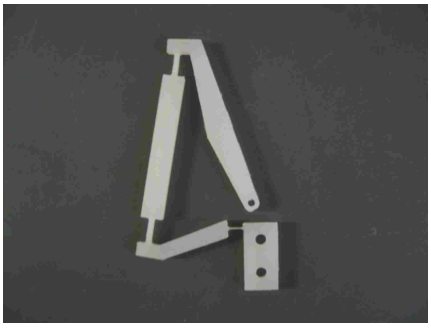

Figure 2.22: Prototype spring designed to approximate a zero-free-length spring.

This method of compliant spring design is accompanied with many limitations, but if used properly it can be a powerful tool in the design of compliant mechanisms. First, the concentrated areas of compliance constituting the torsional springs greatly limit the springs design for an extended range of motion. This is due not only to the PRBM's limitation on the angle of deflection for a flexible member, but also the amount of stress the area experiences. The high stresses that are seen for the springs contribute to the method's limitation in producing higher force or moment springs with a large range of deflection. There are many elements within the PRBM that can be used to reduce this effect (long flexible beams instead of small-length-flexural pivots), but these elements do not guarantee a sufficient reduction in stress throughout the spring design to see

significant increase in the magnitude of the spring's output. Additionally, they may add to the inaccuracy of the model due to the nature of their differing behavior under different loading conditions as described in [15] . While more springs can be implemented to overcome these limitations, the complexity of the model increases for each additional joint.

By using a genetic algorithm to initially explore the design space for the spring many local minima are avoided in the optimization search. However with a design space that has as many variables as these springs contain, it is difficult to ensure a better solution is not achievable. The method as presented performs consistently in generating spring designs that closely approximate a target force-deflection or moment-deflection responses, with the limitations as stated previously, but still has the ability to fall into a local minimum and be unable to climb out to find a more feasible solution. This is in great part due to the complexity of the design space and the objective function that is presented in this work.

The results presented here support that the PRBM for the springs developed above is a suitable method for modeling compliant mechanism springs and their output behavior. Additionally the capability of the optimization routine to search the design space for springs with designs that produce the desired output response is displayed. This data supports the idea that springs can be designed for target outputs and that the outputs can then be crafted so that the resulting designs can be combined with one another and a compliant joint, resulting in a statically balanced mechanism that can be accurately modeled.

CHAPTER 3. DESIGN OF STATICALLY BALANCED COMPLIANT JOINTS (SBCJ)

The spring models and optimization routine are the tools that allow for the design of a SBCJ. The work discussed in the previous chapter is what allows for the joint design to incorporate balancing springs with non-linear loading conditions. It does this by providing approximations of the spring's motion and force/moment output that can be used to achieve the criteria necessary to balance a compliant joint. In this chapter the process by which the SBCJ is designed and how it utilizes the spring optimization methods is presented.

The core of the science of static balancing of mechanisms is the energy levels seen in the system. To maintain a statically balanced state, the energy level in the system needs to be constant, meaning that no energy needs to be added into the system to maintain a particular position. This state of static balancing can be seen as a neutrally stable equilibrium point that extends over the range of motion of the mechanism. Approaches to achieve this constant energy state include working directly with energy in the system, or looking at a newtonian approach where forces and moments acting within the system must be equal to zero over the range of desired static balancing. These two approaches can be applied at a system level or on a component level where individual components are made to compliment each other.

In this work a building block, or piece by piece, approach is taken to design a SBCJ. Here the joint itself is considered and modeled and based on that model two balancing springs are designed so that the entire joint is predicted to display a level of static balancing. The following sections outline the models and methods used in this design procedure that results in a fully compliant statically balanced mechanism that approximates the motion of a rotary joint.

3.1 Model of Compliant Joint and Balancing Equilibrators

The approach taken to achieve a statically balanced compliant joint is based on selecting multiple parameters of the joint design. These include the location of attachment points of the

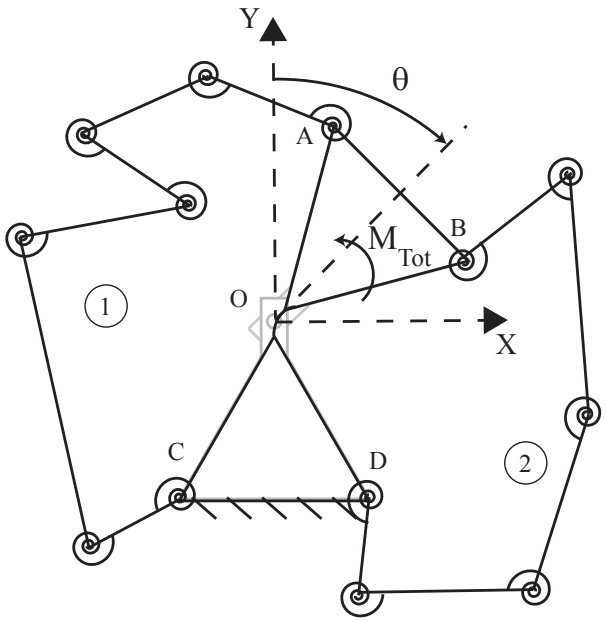

Figure 3.1: Concept for a fully compliant spring butterfly mechanism

spring to the compliant joint that is being balanced. These attachment points define how the spring deflects and the magnitude of the deflection. Also the type of springs implemented in the design of a SBCJ plays a large role. Depending on the type of springs used the designer can be limited to a very small range of attachment points that will result in a SBCJ. By being able to design springs that display moment displacements that will add the necessary energy to the joint to cancel the energy stored in a compliant joint, the criteria of the spring attachment points is less constricted. This capability allows for the spring design to conform to the joint design. The energy that the springs must add can be calculated by investigating the moments present in the compliant joint, as they relate directly to the energy stored in torsional springs. To maintain a state of static balancing the moments exerted on and output from the compliant joint must sum to zero at every point over the desired range. For a compliant spring-butterfly as shown in Fig. 3.1, the moment equation is given by

$$M_{Tot} = T_{joint} + M_{sp_1} + M_{sp_2} = 0, \tag{3.1}$$

where T_{joint} is defined by the type of compliant joint that is implemented, and M_{sp_1} and M_{sp_2} are the moments produced by the balancing springs, which are found using the method presented in Chapter 2.

The steps taken for the design of a SBCJ are as follows.

1. The stiffness of the uncompensated joint is modeled and its motion is quantified. In this case a four-bar model of the cross-axis flexural pivot (CAFP) is implemented to predict the joint's motion and its stiffness.

2. Spring 1 is initially specified to have a linear force-deflection curve given by $k * \delta_{sp}$. The endpoints of spring 1 (points A and C) on the SBCJ are chosen so that the distance between the points is the spring's free-length when $\theta = \theta_{max}$ as shown in Fig. 1.5(a) and $M_{sp_1} = -T_{joint}$ when the $\theta = \theta_{min}$ shown in Fig. 3.2(b).

3. With points A and C defined, the spring design is generated using an optimization method that was developed for the generation of spring designs for prescribed loading conditions. The actual moment modeled by the spring's PRBM is then used to find the target moment for the second spring
$$M_{sp_2} = -(T_{joint} + M_{sp_1}). \tag{3.2}$$

4. The desired moment for the second spring is used as the objective of the optimization and a design for the second spring is obtained using placements of points B and D so that the joint is symmetrical. Figure 1.6 demonstrates what the resulting moments are when the spring designs produce the desired moments.

For this approach accurate models of the compliant joint and the compliant springs are necessary. The compliant joint chosen for the design is the (CAFP) due to its reportedly good off-axis stiffness, and the existence of a detailed model [43].

3.1.1 Cross-Axis Flexural Pivot

The cross-axis flexural pivot is a compliant joint that obtains its motion through the deflection of thin cross members as shown in Fig. 3.3. Previous work has shown that the motion and stiffness of the CAFP can be accurately approximated through the PRBM and FEM approaches [43, 44]. Jensen [43] presented two models of the CAFP that approximated the joint's characteristics. A pin joint model is presented that proves to be able to predict the joint's stiffness well over

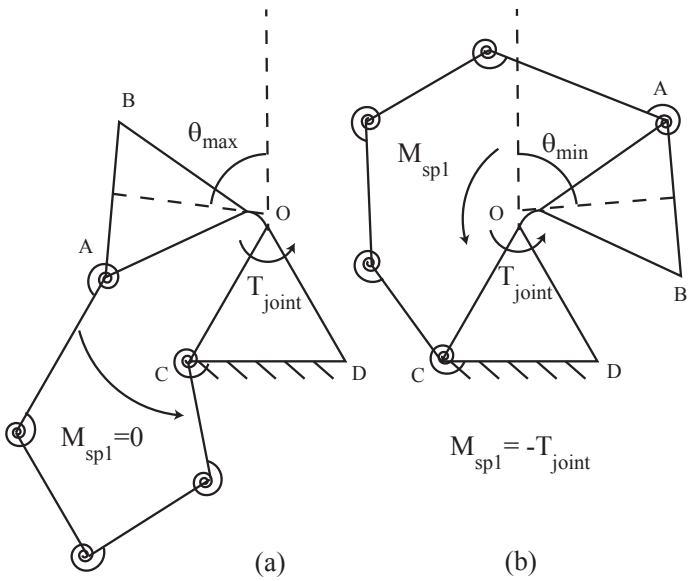

Figure 3.2: Spring 1 attachment on the compliant joint. (a) Attachment position of the undeflected spring 1. (b) Position of the maximum deflection for spring 1

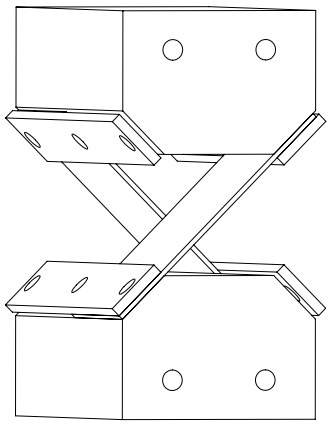

Figure 3.3: A view of a typical configuration of the cross-axis flexural pivot.

a range of $\pm$ 60 degrees. The four-bar model presented by Jensen predicted the stiffness of the CAFP and also its motion very well compared to FEM and experimental results. This four-bar model is the model used to define the joint's stiffness and the path that the attachment points (A, B, C, and D in Fig. 1.5) of the balancing springs will follow in the SBCJ.

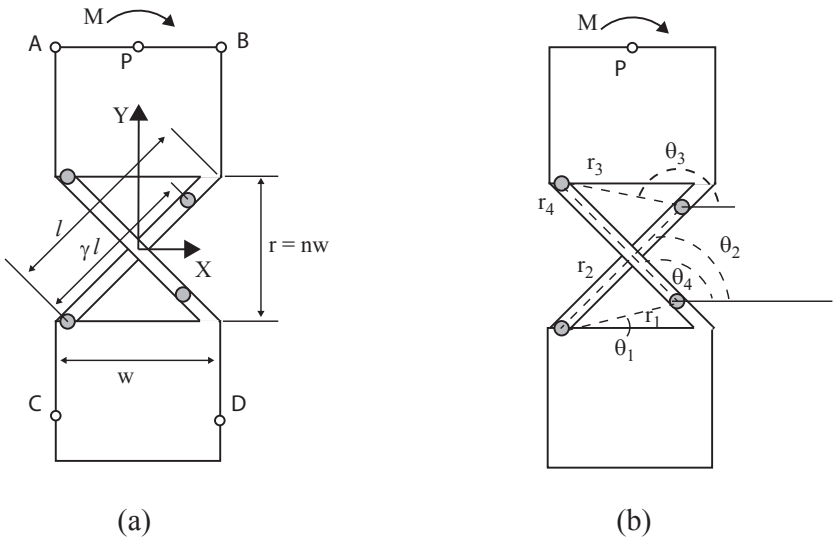

Figure 3.4: The four-bar model for the cross-axis flexural pivot for one direction of rotation.

The four-bar PRBM for the CAFP in Fig. 3.4(b) is a representation for the joint's deflection due to a positive rotation of the coupler link (r_3). The model is to be mirrored for the other half of the joints motion. However, due to symmetry of the joint, the stiffness and motion of the joint for one direction will be representative of its motion for the other. The path that the coupler link follows is found by solving the kinematic equations for the four-bar with the coupler link being the input link. The path of the center of the coupler link is presented in Fig. 3.5. It can be seen that the coupler's path approximates a circle for a good range of the joint's motion. However for this implementation of a SBCJ the attachment points of the springs are not guaranteed to be attached in the midpoint of the coupler link. Rather for the prototype presented in the following sections an attachment point that is 0.02 m off the Y axis and 0.0395 m off the X axis of the undeflected joint as shown defined in Fig. 3.4is implemented. The path that point A follows is shown in Fig. 3.6 along with the path that shows what a circular path of a pin joint would be. It is clearly shown that the path that the springs will follow is not a circular path and that this deviation from a circular path is sufficient enough that the path must be accurately modeled and accounted for when designing the balancing springs for the SBCJ.

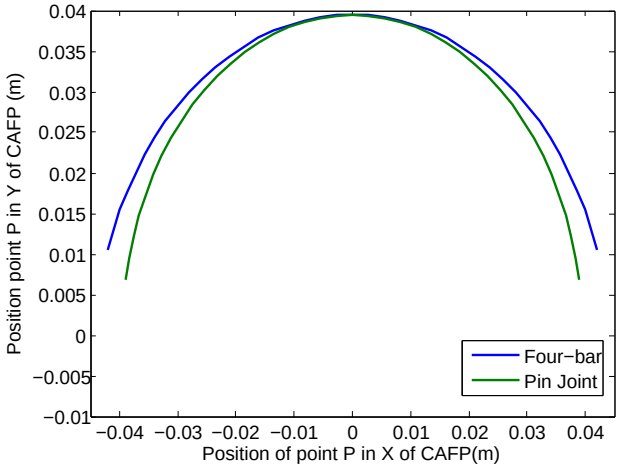

Figure 3.5: The path of point P on the coupler link of the CAFP compared to a pin joint.

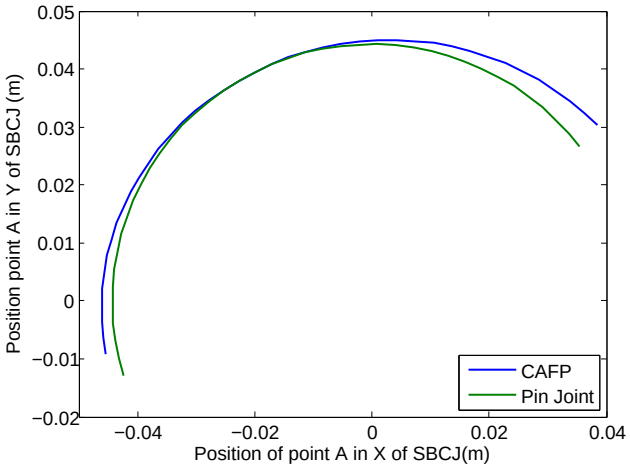

Figure 3.6: The path of point A on the SBCJ based on the motion of the CAFP compared to a pin joint.

The stiffness of the joint is found through the principle of virtual work and the moment required to deflect the joint to a given angle is given by

$$M = T_2 + T_3 - (T_1 + T_2)\frac{r_3 \sin(\theta_3 - \theta_4)}{r_2 \sin(\theta_4 - \theta_2)} - (T_3 + T_4)\frac{r_3 \sin(\theta_3 - \theta_2)}{r_2 \sin(\theta_4 - \theta_2)}, \tag{3.3}$$

Table 3.1: Parameters for the Cross-Axis Flexural Pivot

CAFP Parameter	
n	1
l	2.5 cm
w	1.77 cm
flexure thickness	0.00762 cm

where

$$\begin{aligned} T_1 &= K(\theta_1 - \theta_{1_o}) \\ T_2 &= K(\theta_2 - \theta_{2_o} - \theta_3 + \theta_{3_o}) \\ T_3 &= K(\theta_4 - \theta_{4_o} - \theta_3 + \theta_{3_o}) \\ T_4 &= K(\theta_4 - \theta_{4_o}) \end{aligned} \tag{3.4}$$

and the "o" subscript denotes that they are the undeflected values of the angles of the four-bar. K is calculated using the equation

$$K = \gamma K_{\theta,fb} \frac{EI}{l}, \tag{3.5}$$

where $K_{\theta,fb}$ is found using a curve fit data set. For this study the flexures are set at perpendicular angles to one another, and the value of $K_{\theta,fb}$ was found to be 2.2838. Using these equations, a pivot was designed using 1095 tempered spring steel for the flexures. The parameters for the pivot are given in Table 3.1.

Presented here is an overview of the motion and stiffness of the CAFP and how it affects the design of a SBCJ. This section shows the detail that must be given to the compliant joint modeling in order to be able to design balancing springs to the proper level of accuracy so that the entire assembly of a compliant joint and the balancing springs results in a statically balanced compliant mechanism.

Table 3.2: Spring Attachment Points on the Cross-Axis Flexural Pivot

Attachment Point	X	Y
A	-0.02	0.0395
B	0.02	0.0395
C	-0.02	-0.0395
D	0.02	-0.0395

3.1.2 Balancing Springs

The moment that the balancing springs need to collectively apply to the joint must exactly equal the negative value of the moment required to hold the compliant pivot in place. There are countless combinations of the two spring moments that can result in the cancelation of the restoring torque of the pivot, and choosing a good starting point for the spring optimization proves to be a challenge. Rather than beginning with a wide open field of possible moment displacement curves, the approach taken here is to initially specify the desired moment for the first spring. This is done according to the steps outlined in the beginning of this chapter relating to the specification of the desired moment response and the location of the spring attachments.

The locations of the spring's attachment points on the CAFP that result in the desired target moment for the first balancing spring are found in Table 3.2. Using these values to model the spring's path and displacements, the spring optimization process is completed. Figure 3.7 shows the steps taken in the optimization of the two springs to achieve static balancing. As shown in Fig. 3.7 the desired moment for the first spring is used as the objective of the optimization routine explained in Chapter 2. Upon its completion, the desired moment for the second spring is calculated using

$$M_{sp_2} = -(T_{joint} + M_{sp_1}). \tag{3.6}$$

M_{sp2} is then used as the objective of the optimization for the second spring. At this point a joint design is obtained that, based on the performance of the two optimizations, displays a level of static balancing. Realizing that the use of the genetic algorithm in the optimization process does not guarantee the best design to be found, this process is iterated. However, in the subsequent iterations of the optimization, the desired moment curves for each spring are calculated using the

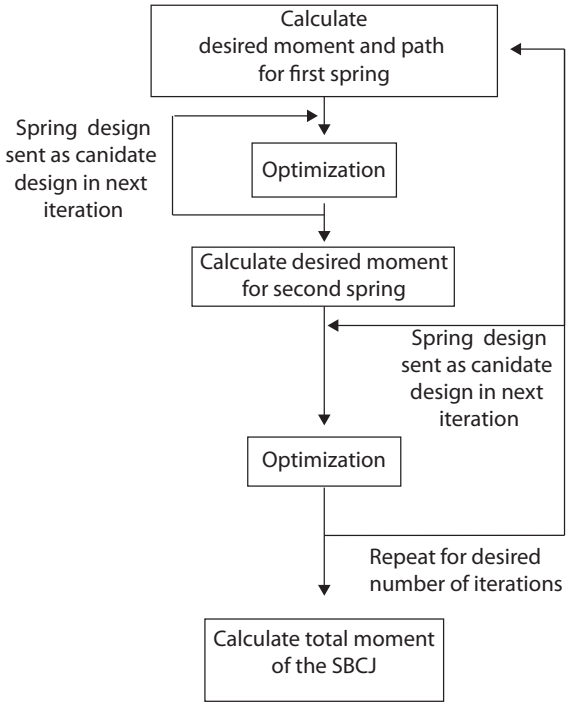

Figure 3.7: A flow chart for the process in which the design for a SBCJ is obtained.

latest design iteration of the opposing balancing spring and the compliant joint. Figure 3.7 shows the process of the optimization of the entire joint. In the uppermost block of Fig. 3.7 the desired moment is calculated for the first spring as described in the opening of this chapter. In the following iterations the desired moment is calculated for the first spring using Eq. 3.7

$$M_{sp_1} = -(T_{joint} + M_{sp_2}). \tag{3.7}$$

In Eq. 3.6 and 3.7 the values of M_{sp_1} and M_{sp_2} are those which are calculated for the most recently found spring design for the balancers.

Additionally, the genetic algorithm is supplied with the previous design for that spring from the previous iteration as one of the members of the population in the first generation of the genetic algorithm. By supplying the previous design it allows the genetic algorithm to further evolve that design into a more optimal solution in the following iterations. This process was repeated 5 times. This number of iterations was chosen because it was observed that the designs tended to converge after the fifth iteration. By using the CAFP, the springs that are generated will not follow

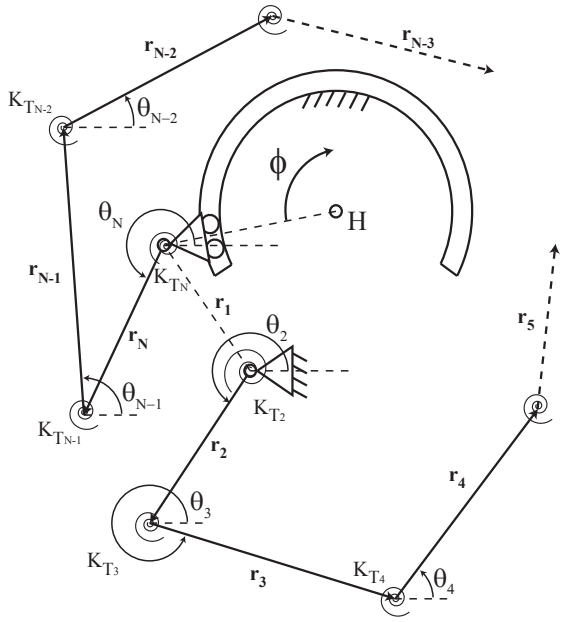

Figure 3.8: The PRBM for a generic compliant mechanism spring

a perfectly circular path. To account for this, the path of the spring shown in Fig. 3.8 is modeled for every angle of θ and is passed to the optimization as the end points of $\mathbf{r_1}$. With these values supplied to the spring optimization algorithm, the non-circular path is properly represented in the minimization of potential energy (Eq. 2.24) that is used to characterize the spring's position.

3.2 Prototype Design

The joint optimization was performed multiple times in an effort to explore more of the joint's design space. From the results that were obtained, the design that resulted in the best combination of the joint's balancing and the levels of stress in the springs was chosen and prototyped. The configurations for the two balancing springs chosen for the design are shown in Fig. 3.9, where points A, B, C, and D correspond to the locations shown in Figs. 3.1 and 3.4. A list of parameters for the spring designs is found in Table 3.3. The candidates not chosen for the final design typically had similar configurations to the springs shown here but with differing link lengths or had one less link. These designs were not chosen for a variety of reasons. These included the range over which

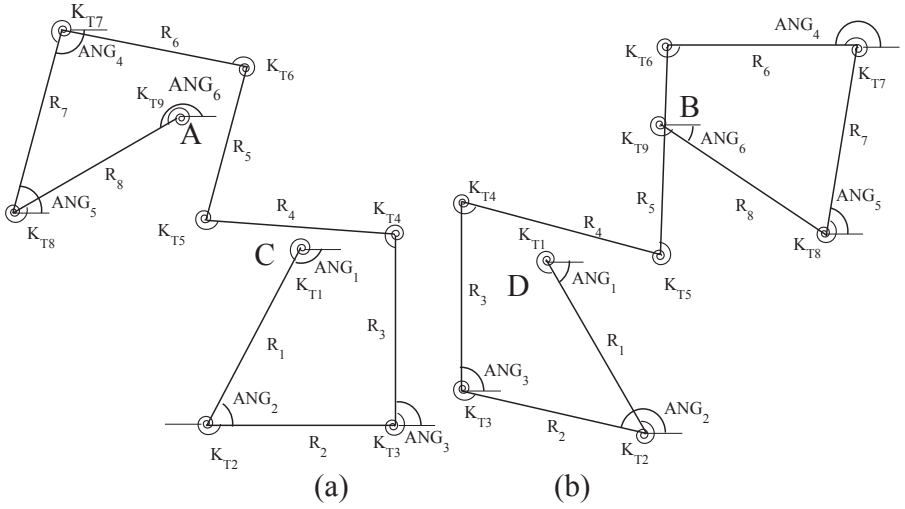

Figure 3.9: Two configurations of the balancing springs. (a) Undeflected spring 1 and (b) represents undeflected spring 2.

Table 3.3: Parameters for the Balancing Springs in the SBCJ

Spring	**ANG** (rad)	**R** (cm)	$\mathbf{K_T}$ Sp. Const.$(\frac{Nm}{rad})$
1	-2.057, 0, pi/2, -0.1963, 1.309, 3.677	4.5, 4.25, 4.25, 4.22, 3.56, 4.25, 4.25, 4.5	0.0375,0.055, 0.0276,0.055, 0.02, 0.055, 0.03521, 0.055, 0.0375
2	5.236, 2.916, pi/2, 3.1416, 1.409, -0.5897	4.5, 4.25, 4.25, 4.616, 4.7, 4.25, 4.33, 4.5	0.0375, 0.02, 0.055, 0.055, 0.02, 0.0322, 0.0212,0.055, 0.0375

static balancing was predicted and if the link lengths configurations in deflected states allowed for the physical space required for the links to not contact one another.

3.3 Fabrication and Testing

A prototype was constructed using spring steel as the flexible segments of the springs and polypropylene as the rigid sections of the springs. Figure 3.10 shows the assembled prototype. The assembled prototype has an approximate footprint of 0.018 m^2. The method of construction and

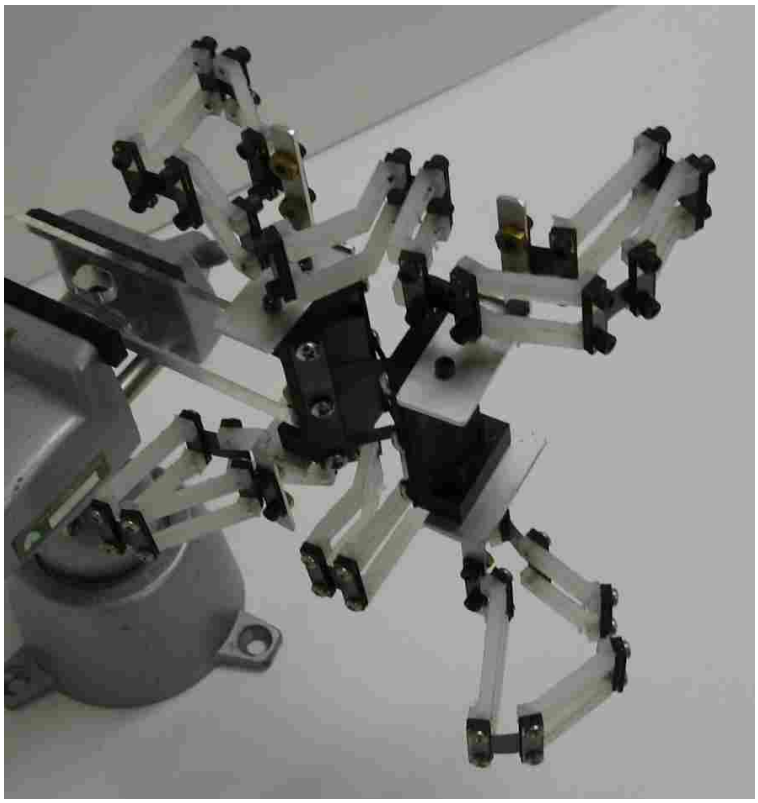

Figure 3.10: The assembled statically balanced compliant joint

materials used was based on modularity and manufacturing limits. By making the springs flexures removable, future work on scaling of the design could be investigated easily with the removal and installation of the flexures. While a spring constructed out of a single piece would have better insured the level of precision in the spring construction, it would have required the entire spring to be constructed out of steel. The weight of the springs was a concern, and thus drove the use of polypropylene and the absence of material from the middle of the rigid links. Additionally, in researching the tolerance limits for the wire EDM process for the available machines, concerns arose over the capability of cutting out sections as thin as was needed in the prototype without losing the whole section or changing the material properties through the excessive heat.

The PRBM predicted moment response and the response as computed by ANSYS finite element modeling (FEM) are shown in Figs. 3.11 and 3.12 for each balancing spring of the SBCJ. It can be seen that the PRBM predictions for the springs that follow a non circular path result in values that align well with the FEM approximations. Additionally the potential energy of each

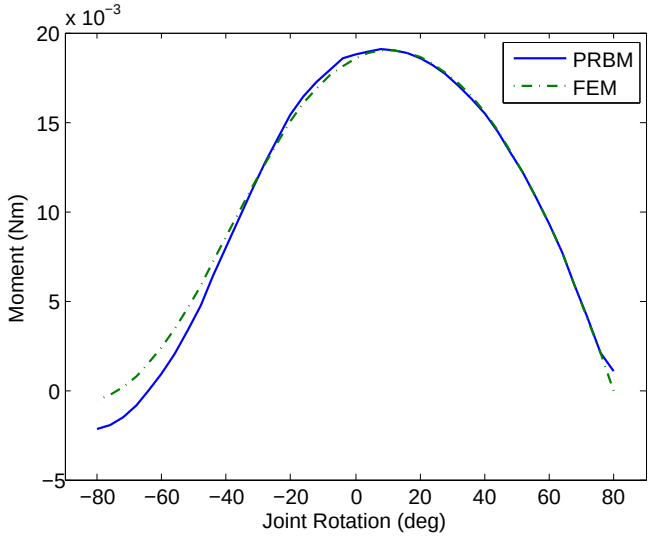

Figure 3.11: Predicted moment response of the first balancing spring

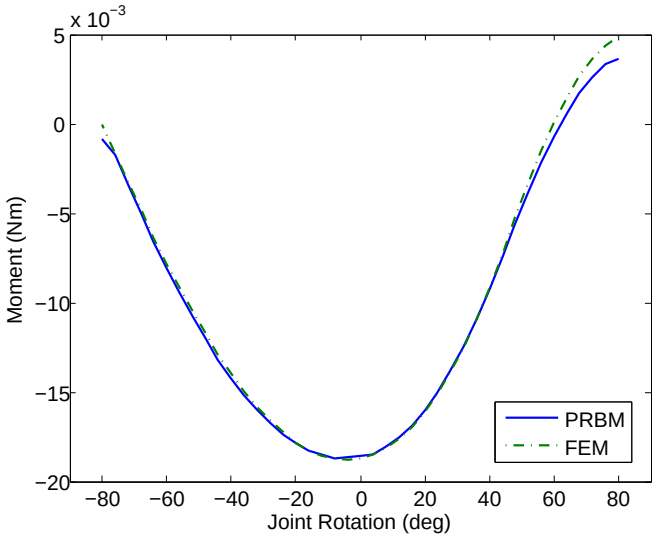

Figure 3.12: Predicted moment response of the second balancing spring

component and the total energy of the assembled SBCJ is presented in Fig. 3.13. This plot shows how the addition of the two balancing springs aides in adding the needed amounts of energy to maintain a constant energy level throughout the range of statically balanced behavior.

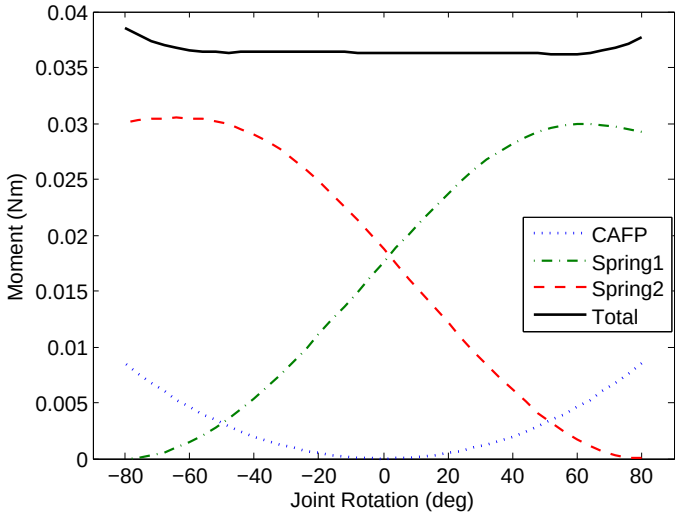

Figure 3.13: Calculated energy storage in the SBCJ

Figure 3.14 displays the total moment for the assembled SBCJ along with the values for the PRBM and FEM approximations. It is seen that the joint is predicted to achieve static balancing over a range of 100 degrees by the method presented and that the FEM results predict a range that is similar to the PRBM predictions. The experimental results show that the prototyped SBCJ in a range of -15 to 10 degrees of rotation of the pivot agrees well with the model presented here. For rotations of the joint for rotations larger than 10 degrees it is seen that the shape of the response trends along a path that is similar to the predicted moment but offset a certain amount. In joint rotation ranges less than -10 degrees the experimental results do not agree well with the FEM or the PRBM approximations, but still displays a reduced moment that is fairly constant through that range.

As seen in Fig. 3.14, the assembled joint's total moment rises and then levels off as it deflects away from the center of the joint. These results seem to suggest some error in the construction of the assembly that causes these offsets of the moments from the predicted values. One possible source of this error is in the tolerances on the lengths of the springs and the boundary conditions at the flexures of the springs. Also the variability in each flexures height and width may not have had a significant effect individually, but as the assembly contains over 22 flexures, the sum of these small tolerances may have become significant. Lastly, in fixing the flexures into place additional

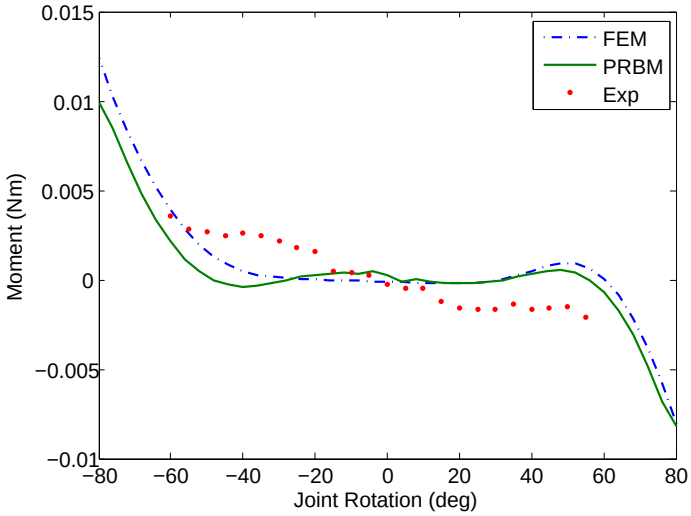

Figure 3.14: The predicted and experimental moment responses of the SBCJ

stresses or loads may be induced. This was especially apparent in the CAFP. In the assembling the CAFP, great care had to be taken in how each flexure was fastened and the level in which the each fastening screw was tightened. If the screws were tightened unevenly, the flexures in the CAFP would display lateral deflections with high compressive loading and pop or snap through a change point into a new deflection configuration.

Though the assembled joint did not display this behavior, the loading may have still been present. The sudden rises in the moment shown in Fig. 3.14 may possibly be attributed to these loading conditions. If this additional loading is present, when the beam changes to a new configuration it may alter the stiffness of the joint, thus the sudden increase of the overall stiffness followed by the more gradual rise in the moment magnitude. Another possible source of this error is that the weight of the springs on the joint have have induced such a behavior by loading the flexures in the CAFP in a way that accentuated this behavior.

The joint was not tested outside of the range of ± 60 degrees due to the pivot beginning to deflect out of the horizontal plane. As the joint rotated out to those larger deflections the weight of the springs began to cause the flexures in the pivot to twist, causing the pivot to sag. This is one adverse consequence to the use of compliant mechanism springs that utilize rigid links.

As the SBCJ was handled and prepared for testing, it was seen that the springs themselves displayed dynamic responses to the motion of the joint. These oscillations occurred while the joint was rotated through its range of motion and as the entire joint was transported and moved through motions it would experience if implemented into a mechanism. The oscillations would die out after 10-15 seconds. From this observation it is clear that the mass of the rigid links is large enough in comparison with the stiffness of the spring that the natural frequency of the spring was not sufficiently high to make the springs unresponsive to the frequencies induced by moving the joint.

The mass of the rigid links was large enough to make the effect of gravity on them as a whole very apparent. As discussed above, the mass of the springs caused the joint to deflect out of the horizontal plane when it would undergo large rotations. With both of these effects present the application of the joint as it is currently designed is very limited. However, it's construction and performance gives great insights on the underlying problems that need to be addressed in order to formulate SBCJs that will be useful in the design of haptic interfaces for increased transparency.

Due to the compliance being concentrated at narrow points within the springs there is great potential for stresses to exceed the yield strength. For this reason the method is limited in its ability to generate designs to compensate for much larger joint moments and still allow for a reasonably sized joint. Additionally, as discussed in Chapter 2, the stress limiting does not bound the width that the flexures can be. In the final design of the SBCJ the flexures implemented resulted in flexures that are longer than the suggested length for a small-length flexural pivot. This was done because the widths chosen by the algorithm were highly variable and at times unrealistic for implementation in the SBCJ. This makes the assumptions made by the PRBM not as accurate and thus is one source of error that can be attributed to the inaccuracy of the model for the final prototype.

Additional error can be attributed to the manufacturing and assembly of the SBCJ. Though great care was taken in the manufacturing and assembly process, tolerances and inaccuracies in the alignment of the flexures most likely occurred. For future implementations of the springs other manufacturing processes will be explored to decrease the complexity of the assembly.

The joint presented here represents advances in several areas in comparison to previous work on SBCJs. One of the major reductions is the foot print of the fully compliant joint design. While it is still large, the method allows for the springs to wrap around the joint which lessens the

width of the joint. This improvement is beneficial in robotic applications especially, as the joints often need to be compact. Scaling of the current design would make it easier for compact joint designs that meet this criteria. Also, this work has provided a method on which specific spring designs can be modeled to meet the designs of the joint. The spring attachment points do not need to be specified to generate the initial target moment response if the moment response that is desired is known or another response is the preferred starting point. This process was solely done to give a starting point for the optimization that would allow for the first optimization to attempt to follow a linear path defined by the relationship $k\delta_{sp}$. Not being constrained to a certain spring design allows for joints to be designed with attachment points that are convenient or conducive to the design, and then the springs can be optimized around that design. In past work the specific spring designs are chosen and optimized. The added flexibility gained from not being constrained to a specific design will allow for future designs of SBCJs to be more freely explored.

CHAPTER 4. CONCLUSIONS AND RECOMMENDATIONS

4.1 Conclusions

The field of static balancing of compliant mechanisms is a growing field that has shown great potential. One area that may benefit by their further development is that of haptic interfaces. The absence of friction, backlash, and no need to compensate for the return-to-zero behavior of the joint will greatly assist in improving the realistic nature of the interface.

In this work, a method for the design of compliant mechanism springs that can be used in the balancing of compliant joints is presented. This method includes a PRBM for the compliant mechanism springs, an approach to modeling their output forces or moments, and an optimization routine that allows for the springs to be designed to follow prescribed force or moment deflection paths. This method was validated through the use of finite element modeling (FEM) software and prototype springs made of polypropylene.

The method for the spring design is then implemented in the design of a statically balanced compliant joint (SBCJ). A process for the design is presented in which the spring attachment points are specified to give a starting objective moment for the spring design and then the spring designs are optimized using the optimization techniques presented here. The design process resulted in a design of a SBCJ that is predicted by the PRBM to have a range of 100 degrees of static balancing. A prototype of the SBCJ was manufactured and experimental data was taken to validate the results of the model. While the actual moment required to deflect the spring does not exactly match over the entire range of motion, overall the prototype displayed a level of moment reduction on the compliant joint that gives confidence in the model and its ability to produce SBCJs. Additionally, it was observed that the spring's mass plays a significant role in the range of deflection the joint can undergo. The mass is also significant in that it reduces the spring's natural frequency into the range of the target input frequencies, resulting in unwanted oscillations.

In summary, the contributions of this research in the areas of the design of statically balanced compliant joints and haptic interfaces are as follows:

- A prototype compliant haptic interface was developed as a case study for the feasibility of the use of compliant parts in haptic interfaces. The prototype displays good static balancing and is capable of providing a small level of force feedback to the user.

- A PRBM was developed for the modeling of compliant mechanism springs that undergo translational deflections and a separate model of springs that follow a prescribed path. The model is general in that it can be expanded to contain as many links as is needed to obtain the functionality that is desired.

- An optimization algorithm that meshes a genetic algorithm with a gradient based search optimization to find spring designs that follow prescribed loading conditions was developed. The algorithm includes functions that penalize designs that exhibit geometry, stresses, or deflections that do not allow for the spring to perform as desired. The designs produced by the algorithm were manufactured and showed predicted levels of force or moments.

- A process to design a statically balanced joint was formulated that utilizes the aforementioned spring models and optimization routine. The process is shown to be successful in that designs for statically balanced joints are produced that match results from finite element modeling software.

- A physical prototype of the compliant joint and both balancing springs was manufactured. The entire assembly constitutes the design of a statically balanced joint. The joint is shown to exhibit output moments of given rotations that supports the model's predicted values with some deviations.

- Two papers covering portions of this work were accepted for publication. One was accepted in the 2010 ASME Dynamics Systems and Controls Conference and the other in the 2011 ASME International Design Engineering Technical Conference.

- A journal article covering portions of this work has been submitted for publication to the ASME Journal of Mechanical Design.

4.2 Recommendations

The work presented here has laid a foundation of work for the application of statically balanced joints in haptic interfaces. Through this work a great deal was learned regarding the limitations and potential applications of SBCJs.

Presented here was a model for compliant mechanism springs using the PRBM. Future work in this area should include investigations on how the number of links contained in the springs and their initial orientation affect the types of displacement curves that the springs can obtain. This would include studies on how differing mechanical advantage in the spring changes the overall stiffness and what limits exist on the stiffness that can be obtained by optimizing this parameter in the spring design.

In conjunction with these studies of the compliant mechanism springs, work needs to be done to investigate ways to lower the weight of the springs. As displayed in the prototype, the weight of the springs not only was a factor in the off-axis stiffness of the joint, but also the added mass on the springs introduced new dynamics into the system. Work in this area may include the study of miniaturization of the total joint design and design principles that can be followed to ensure minimal weight of the springs.

Other modeling techniques for the design of SBCJs for use in robotic applications should be explored and applied to the process for the design of SBCJs presented here. This would include the use of topology optimization methods that will result in spline-like springs with the necessary stiffness and displacement properties. These spline like springs may allow for greater deflections as the stresses present in them will be distributed throughout the entire structure. Also there is potential for the designs to be more compact than those that require rigid segments.

Work related to the direct implementation of SBCJs into haptic interfaces should include studies and tests of other compliant pivots that may be used. In haptics the off axis stiffness is critical to the accuracy of the positions that the interface believes it is displaying. Formulating some metric of off-axis stiffness of the joint's entire range is needed. This metric will allow haptic interface designers to understand the level of compliance that they are encountering by implementing the compliant joint and for the future design of compliant joints with increased off axis stiffness.

With the currently constructed joint, studies can be performed to quantify its dynamic behavior. The study presented here is a static study and the dynamics of joint are not considered. From these studies the researches can look to quantify the natural frequency of the springs. This frequency for the springs can be studied in respect to the spring design to see how the designs can be altered to generate springs that are not responsive to low frequency vibrations (higher natural frequency). In addition to this an additional cost function may be implemented into the optimization to allow this parameter to affect the design. This work would aid the field of SBCM in robotics as it can allow the designers to design spring compensating configurations with compliant mechanisms that do not introduce unwanted dynamics into the system.

Lastly, future work will include the implementation of the current SBCJ design or some future iteration into a haptic interface. This interface can then be used to explore and quantify the effects that the SBCJ has on the haptic interfaces transparency and force feedback characteristics. Included in this work will be specifically designed control schemes that capitalize on the joint's dynamics.

REFERENCES

[1] R. D. P. Fischer and K. Siva, "Specification and design of input devices for teleoperation," in *Proceedings ofIEEE International Conference on Robotics and Automation*, 1990, pp. 540–545. 2, 5

[2] J. E. Colgate and J. M. Brown, "Factors affecting the z-width of a haptic display," in *Proceedings on the IEEE International Conference on Robotics and Automation*, 1994. 2, 5

[3] L. Y. L. D. A. Lawrence and S. Aphanuphong, "Bow spring/tendon actuation for low cost haptic interfaces," in *First Joint Eurohaptics Conference and Symposium on Haptic Interfaces for Virtual Environment and Teleoperator Systems*, 2005. 2, 3, 6

[4] F. H. R. B. Gillespie, T. Shin and B. Trease, "Automated characterization and compensation for a compliant mechanism haptic device," *IEEE/ASME Transactions on Mechatronics*, vol. 13, no. 1, pp. 136–146, February 2008. 3, 6

[5] T. H. Massie and J. K. Salisbury, "The phantom haptic interface: A device for probing virtual objects," in *Proceedings of the ASME Winter Annual Meeting, Symposium on Haptic Interfaces for Virtual Environment and Teleoperator Systems*, 1994. 3, 5

[6] B. D. A. K. L. Steger and H. Kazerooni, "Design of passively balanced spatial linkage haptic interface," *Journal Mechanical Design*, vol. 126, November 2004. 3, 5

[7] A. Carr, "Position Control Comparison of Equilibrate and Mass Counterweight Systems," MS Thesis, Dept. of Mech. Eng., Virginia Polytechnic Institute and State University, 2001. 4, 6

[8] J. L. Herder and F. P. A. van den Berg, "Statically balanced compliant mechanisms (SBCM'S), and example and prospectus," in *Proceedings of the ASME Design Engineering Technical Conference*, 2000. 4, 6, 7

[9] T. A. Kern, *Engineering Haptic Devices*. Springer, 2009. 5

[10] O. K. B. Siciliano, Ed., *Haptics*. 5

[11] J. E. C. D. W. Weir and M. A. Peshkin, "Measuring and increasing z-width with active electrical damping," in *Proceedings of Symposium on Haptic Interfaces for Virtual Environments and Teleoperator Systems*, 2008, pp. 169–175. 5

[12] S. T. McJunkin, "Transparency improvement for haptic interfaces," Ph.D. dissertation, Rice University, May 2007. 5

[13] E. P. K. Vlachos and D. N. Mitropoulos, "Mass/inertia and joint friction minimization for a low-force five-dof haptic device," in *Proceedings of the IEEE International Conference on Robotics and Automation*, 2004, pp. 286–291. 5

[14] K. Vlachos and E. Papdopoulos, "Transparency maximization methodology for haptic devices," *IEEE/ASEM Transactions on Mechatronics*, vol. 11, no. 3, pp. 249–255, June 2006. 5

[15] L. L. Howell, *Compliant Mechanisms*. New York, NY: John Wiley and Sons, 2001. 6, 13, 15, 20, 23, 37, 44

[16] S. O'Modhrain and R. B. Gillespie, "The moose: A haptic user interface for blind persons," in *Proceedings of the of the Third WWW6 Conference*, 1997. 6

[17] K. Hain, Ed., *Spring Design and Application*. 6

[18] J. L. Herder, "Energy-free Systems; Theory, Conception and Design of Statically Balanced Spring Mechanisms," PhD Thesis, Deflt University of Technology, Netherlands, 2001. 6, 7, 9, 17

[19] D. Streit and B. Gilmore, "Perfect spring equilibrators for rotatable bodies," *ASME Journal of Mechanisms, Transmissions, and Automation in Design*, vol. 111, pp. 451–458, December 1989. 6

[20] D. Streit and E. Shin, "Equilibrators for planar linkages," in *Proceedings of the ASME Mechanisms Confernece*, 1990, pp. 21–28. 6

[21] C. M. Gosselin, "Static balancing of spherical 2-dof parallel mechanisms and manipulators," *International Journal of Robotics Research*, vol. 18, no. 8, pp. 819–829, 1989. 6

[22] E. H. F. Riele and J. Herder, "Planar and spatial gravity balancing with normal springs," in *Proceedings of the ASME Design Engineering Technical Conference*, 2004. 6

[23] P. G. A. Gopalswamy and M. Vidyasagar, "A new parallelogram linkage configuration for gravity compensation using torsional springs," in *Proceedings of the IEEE International Conference on Robotics and Automation*, 1992. 6

[24] W. D. B. W. R. Barents, M. Schenk and J. Herder, "A new parallelogram linkage configuration for gravity compensation using torsional springs," in *Proceedings of the ASME International Design Engineering Technical Conference*, 2009. 6

[25] F. M. Morsch and J. L. Herder, "Design of a generic zero stiffness compliant joint," in *Proceedings of the ASME International Design Engineering Technical Conference*, 2010. 7, 9

[26] J. A. G. G. Radaelli and J. L. Herder, "An energy approach to static balancing of systems with torsion stiffness," in *Proceedings of the ASME International Design Engineering Technical Conference*, 2010. 7, 9

[27] J. A. Gallego and J. L. Herder, "Synthesis methods in compliant mechanisms: An overview," in *Proceedings of the ASME International Design Engineering Technical Conference*, 2009. 7

[28] V. A. H. N. Tolou and J. L. Herder, "Statically balanced compliant micro mechanisms (sbmems): Concepts and simulation," in *Proceedings of the ASME International Design Engineering Technical Conference*, 2010. 7

[29] B. D. Jensen and C. H. Jenkins, "Design of small-scale statically balanced compliant joints," in *Proceedings of the ASME International Design Engineering Technical Conference*, 2011. 7, 9

[30] J. A. Gallego and J. L. Herder, "Criteria for the static balancing of compliant mechanisms," in *Proceedings of the ASME International Design Engineering Technical Conference*, 2010. 7

[31] C. K. K. Hoetmet, G. Woo and J. L. Herder, "Negative stiffness building bocks for statically balanced compliant mehanisms: Design and testing," in *Proceedings of the ASME International Design Engineering Technical Conference*, 2010. 7

[32] Associated Spring Corp., *Springs, a Bibliography*. Bristol, CT: Associated Spring Corp., 1957. 7

[33] B. T. Edwards, B. D. Jensen, and L. L. Howell, "A pseudo-rigid-body model for functionally binary pinned-pinned segments used in compliant mechanisms," in *Proceedings of the ASME Design Engineering Technical Conference*, 1999. 8

[34] L. L. Howell, A. Midha, and M. D. Murphy, "Dimensional synthesis of compliant constant-force slider mechanisms," in *Proceedings of the ASME Design Engineering Technical Conference*, 1994. 8, 9

[35] J. J. Parise, L. L. Howell, and S. P. Magelby, "Ortho-planar linear-motion springs," *Mechanism Machine Theory*, vol. 36, pp. 1281–99, 2001. 8

[36] C. V. Jutte and S. Kota, "Design of nonlinear springs for prescribed load-displacement functions," *ASME Journal of Mechanical Design*, vol. 130, no. 081403, August 2008. 8

[37] ——, "Design of single, multiple, and scaled nonlinear springs for prescribed nonlinear responses," *ASME Journal of Mechanical Design*, vol. 132, no. 011003, January 2010. 8

[38] M. B. Parkinson, L. L. Howell, and J. J. Cox, "A parametric approach to the optimization-based design of compliant mechanisms," in *Proceedings of the ASME Design Engineering Technical Conference*, 1997. 8

[39] C. B. W. Pedersen, N. A. Fleck, and G. K. Anathasuresh, "Design of a compliant mechanism to modify an actuator characteristic to deliver a constant output force," *ASME Journal of Mechanical Design*, vol. 128, no. 5, pp. 1101–1112, 2006. 9

[40] L. L. Howell and A. Midha, "A method for the design of compliant mechanisms with small-length flexural pivots," *Journal Mechanical Design*, vol. 116, March 1994. 13

[41] B. D. J. Q. T. Aten, S. A. Zirbel and L. L. Howell, "A numerical method for position anslysis of compliant mechanisms with more degrees of freedom than inputs," *Journal Mechanical Design*, vol. 133, June 2011. 28

[42] S. C. Chapra and R. P. Canale, *Numerical Methods for Engineers*. McGraw-Hill. 31

[43] B. Jensen and L. Howell, "The modeling of cross-axis flexural pivots," *Mechanism and Machine Theory*, vol. 37, no. 5, pp. 461–476, May 2002. 47

[44] Z. Hongzhe and B. Shusheng, "Stiffness and stress characteristics of the generalized cross-spring pivot," *Mechanism and Machine Theory*, vol. 45, pp. 378–391, 2010. 47